ELSEVIER

Journal of Nuclear Materials 282 (2000) 1–31

journal of nuclear materials

www.elsevier.nl/locate/jnucmat

Review

Fuel corrosion processes under waste disposal conditions

D.W. Shoesmith

Department of Chemistry, The University of Western Ontario, London, Ont., Canada N6A 5B7

Received 20 July 1999; accepted 25 July 2000

Abstract

The release of the majority of radionuclides from spent nuclear fuel under permanent disposal conditions will be controlled by the rate of dissolution of the UO_2 fuel matrix. In this manuscript the mechanism of the coupled anodic (fuel dissolution) and cathodic (oxidant reduction) reactions which constitute the overall fuel corrosion process is reviewed, and the many published observations on fuel corrosion under disposal conditions discussed. The primary emphasis is on summarizing the overall mechanistic behaviour and establishing the primary factors likely to control fuel corrosion. Included are discussions on the influence of various oxidants including radiolytic ones, pH, temperature, groundwater composition, and the formation of corrosion product deposits. The relevance of the data recorded on unirradiated UO_2 to the interpretation of spent fuel behaviour is included. Based on the review, the data used to develop fuel corrosion models under the conditions anticipated in Yucca Mountain (NV, USA) are evaluated.

1. Introduction

The predominant form of high level nuclear waste available for disposal is the spent fuel bundle discharged from reactor. While the prospects for the development of long-lived nuclear waste containers are promising [1], their failure will eventually lead to the formation on the fuel surface of the wet, potentially oxidizing conditions which could lead to fuel degradation and the release of radionuclides. If the release of these radionuclides is to be predicted, and overall repository performance assessed, then a clear understanding of potential fuel degradation process is required.

Over the past 20 years or more a substantial effort has been expended to study fuel dissolution and radionuclide release processes under a range of proposed waste vault/repository conditions. A review of the early understanding has been published [2]. The present report will summarize the basic chemistry of UO_2 and how this is affected by factors expected to influence fuel corrosion under waste vault/repository conditions. These factors are the intrinsic corrosion rate, pH, O_2 concentration, HCO_3^-/CO_3^{2-} concentration, temperature, water radiolysis, other potential ground water constituents (especially Ca^{2+}, SiO_4^{4-}), the relative reactivities of unirradiated UO_2 and spent fuel (including in-reactor burn up), and the formation of secondary phases and their ability to trap radionuclides. Subsequently, the database compiled to predict the performance of spent fuel waste forms in the Yucca Mountain (NV, USA) repository will be assessed in the light of this general understanding. This database is compiled and discussed in the Waste Forms Characterization report [3].

2. Basic fuel properties

Commercial nuclear fuel is basically uranium dioxide (UO_2) (natural or enriched) fabricated by sintering pressed compacts of very fine-grained powder at ~1700°C under a reducing atmosphere. These sintered ceramics typically have 92–99% of the theoretical density with grain sizes of 2–15 μm. The as-fabricated fuel is a slightly hyperstoichiometric oxide, UO_{2+x}, where $x \leqslant 0.001$. The presence of excess oxygen, as interstitial ions (O_I^{2-}), requires further ionization of a small fraction of the U^{IV} ions, to the U^{V} and/or U^{VI} valence states, leading to the creation of holes in the narrow occupied U5f sub-band. These holes can migrate by a small polaron-hopping process with a low activation energy, and confer a moderate conductivity on the oxide. The band

0022-3115/00/$ - see front matter
PII: S0022-3115(00)00392-5

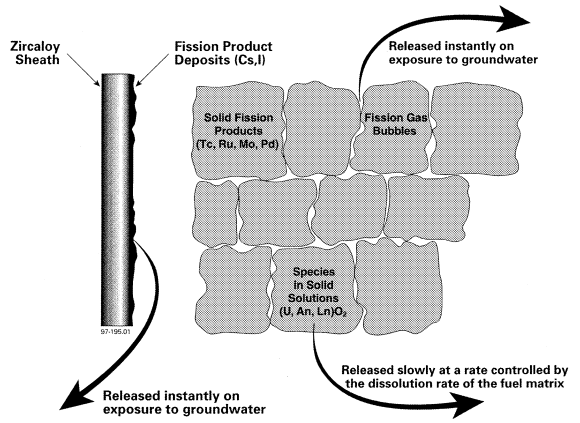

Fig. 1. Schematic diagram showing the distribution of radionuclides in used fuel. Radionuclides located at the fuel–Zircaloy cladding gap and at grain boundaries within the fuel are assumed to be instantly released.

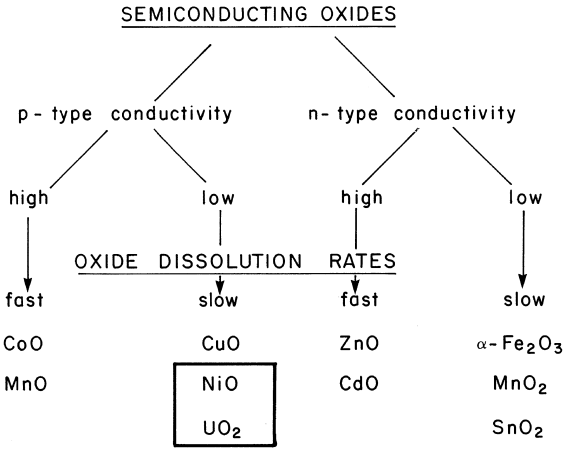

Fig. 2. Categorization of oxides according to their conductivity type and dissolution behaviour [5].

structure and conductivity of UO_2 have been reviewed [4].

On burning the fuel in-reactor, many fission products and actinides with widely varying solubilities in the host matrix are created. These radionuclides can be separated into a number of distinct categories, Fig. 1:

1. Fission products (Cs, I) which separate to the fuel sheath gap.
2. Fission products which migrate to grain boundaries in the fuel to occupy either fission gas bubbles or solid fission products such as perovskites ((Ba, Sr)ZrO_3) and the metallic ε-phase (Mo, Ru, Rh, Pd, Tc).
3. Fission products and actinides and lanthanides that are retained in the fuel matrix.

The great majority of radionuclides (>90%) are in category (3) and are expected to be released at a rate governed by the dissolution (corrosion) rate of the uranium oxide matrix. The release rate of those radionuclides in category (2) will also be controlled, to some degree, by fuel matrix degradation processes.

3. Corrosion of UO_2

3.1. Electrochemical behaviour

3.1.1. General electrochemical features

The parameters which control the dissolution rates of oxides have been reviewed by [5]. A characteristic of oxide dissolution processes is the wide range of rates, which can vary by many orders of magnitude, even for the same oxide. For slowly dissolving semiconducting oxides, the category to which unoxidized UO_2 fits, Fig. 2, the rate-controlling process is either charge transfer to the surface to form surface ionic species (M^{n+}, O^{2-}) which can subsequently transfer to solution, or surface alterations to produce these transferrable ionic species. Thus, properties such as solid-state conductivity, ion formation at surface defect sites, and the solution redox potential are major factors that determine the kinetics of dissolution.

For UO_2, the solution redox potential is the critical variable, since the solubility of UO_2 increases by many orders of magnitude when the solid is oxidized, Fig. 3. Reaction with an oxidant (e.g. O_2) can be considered as the injection of a hole into the U5f band, which will increase the conductivity on the oxide surface as well as produce the solution soluble UO_2^{2+} species [4]. This sensitivity to oxidation makes fuel dissolution, and the release of radionuclides, dependent on repository redox conditions. Consequently, it is necessary to treat fuel dissolution as a corrosion process.

The redox potential ($E_{OX/RED}$) for most oxidizing agents expected in a repository will be more positive than the equilibrium potential, ($E_{UO_2^{2+}/UO_2}$) for the oxidative dissolution of the fuel, Fig. 4, and corrosion of the fuel will proceed at the corrosion potential (E_{CORR}) established at the fuel/environment interface. For normal aerated conditions, the equilibrium potentials for a range of fuel oxidation reactions (to $U_4O_9, U_3O_7, U_3O_8, UO_3 \cdot 2H_2O$) are well below E_{CORR} and complex surface chemistry would be anticipated as fuel corrosion progresses, Fig. 5.

In the sealed vaults anticipated under granitic conditions [6], the equilibrium potential for the fuel will increase and $E_h(\equiv E_{OX/RED})$ of the environment decrease, since the amount of available oxidant is limited. As oxidants are consumed, E_h will approach the H_2O/H_2 potential boundary, Fig. 5, and UO_2 would become the stable matrix. For these conditions the driving force for fuel dissolution would be proportional

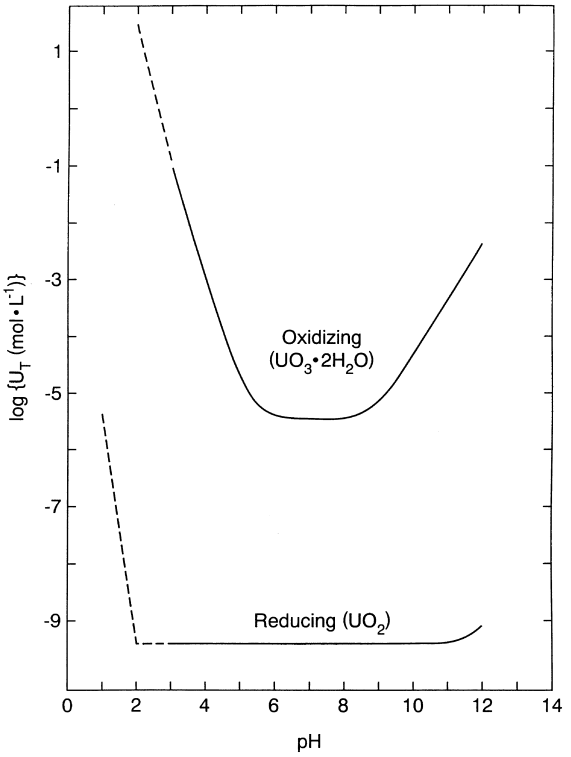

Fig. 3. Solubilities of uranium dioxide (UO_2) and schoepite ($UO_3 \cdot 2H_2O$) as a function of pH at 25°C [4].

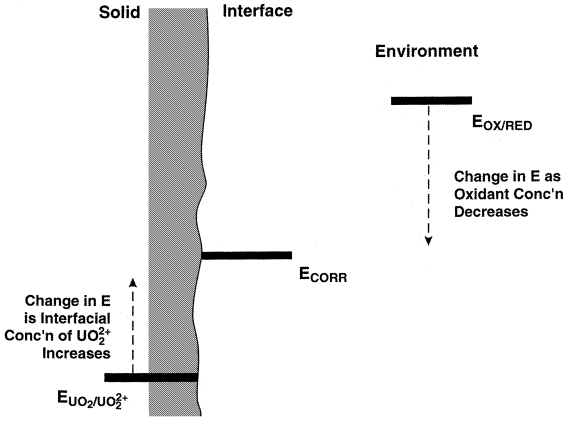

Fig. 4. Relationship between potentials when the surface of nuclear fuel is not at equilibrium with its environment, and an electrochemical driving force for corrosion exists.

to UO_2 solubility, and the rate of dissolution would be controlled by processes such as those described by Segall et al. [5], and discussed above. For unsealed vaults such as Yucca Mountain, where oxidizing conditions can prevail indefinitely, $E_{OX/RED}$ will not decrease with time and the driving force for corrosion will be maintained.

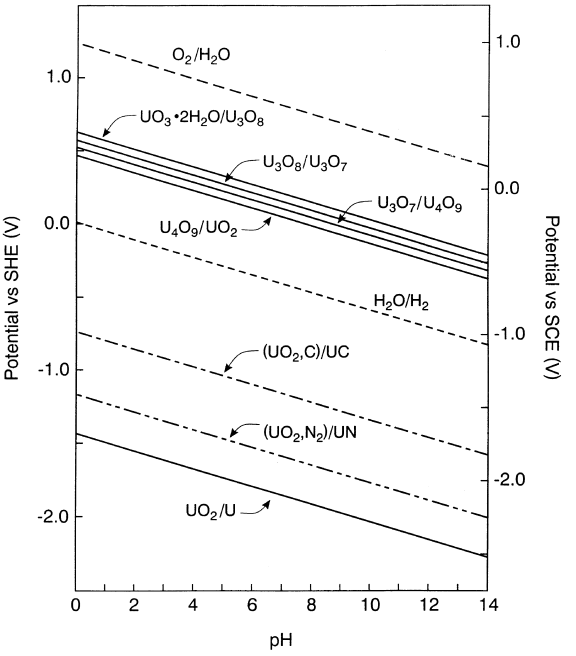

Fig. 5. Potential–pH diagram showing the relative stabilities of uranium phases potentially stable under fuel corrosion conditions. Although the stability lines for uranium metal, carbides and nitrides are also shown they are not relevant to the present discussion [4].

A second major potential source of oxidants to drive the corrosion of fuel is water radiolysis. Fig. 6 shows the alpha, beta, gamma dose rates calculated at the fuel surface [7]. While the dose rates shown are for a CANDU fuel bundle (burnup, 721 GJ (kg U)$^{-1}$; 10 years since discharge from reactor), similar profiles would be obtained for an LWR bundle. It is worth noting that the

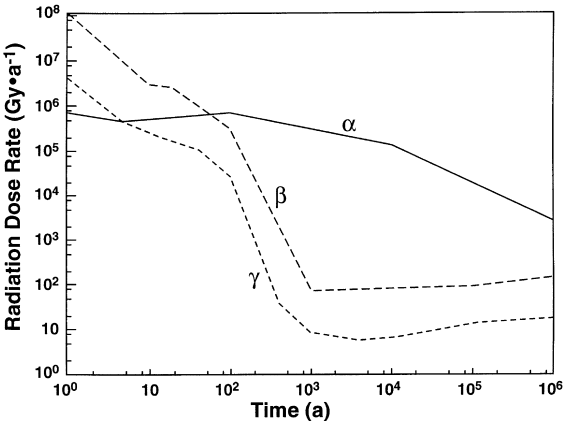

Fig. 6. Alpha (α), beta (β), and gamma (γ) dose rates in the water layer in contact with a CANDU fuel bundle with a burnup of 721 GJ/KgU as a function of time [7].

concentration of radiolytic oxidants will not necessarily be independent of environmentally established redox conditions. The presence of dissolved O_2 while radiation fields endure (particularly β/γ fields) will lead to a significant increase in the production of radiolytic oxidants. Also, if radiolysis of a moist air environment occurs, radiolytic processes leading to the fixation of nitrogen (as NO, NO_2) and the development of acidity (HNO_3) are possible [8]. The presence in the repository of alternative sinks for the reduction of radiolytic oxidants, such as carbon steel waste package liners or the inner walls of a copper container, could significantly reduce the concentration of oxidants available to drive fuel corrosion [9–11].

The corrosion potential, E_{CORR}, is determined by the kinetic balance of the anodic

$$UO_2 \rightarrow UO_2^{2+} + 2e \quad (1)$$

and cathodic

$$Ox + 2e \rightarrow Red \quad (2)$$

reactions which make up the overall corrosion reaction, Fig. 7. At E_{CORR}, the anodic current, I_A, is equal and opposite in sign to the cathodic current, I_C and equal to the corrosion current, I_{CORR}. The value of I_C is the sum of the individual currents for all the oxidant reduction reactions supporting fuel corrosion (i.e. $I_C = I_{C1} + I_{C2}$ in Fig. 7). Using Faraday's Law, I_{CORR} can be expressed as a rate of mass loss,

$$\frac{W}{t} = \frac{I_{CORR} A_W}{nF}, \quad (3)$$

where W is the mass loss in grams, A_W the molecular weight of UO_2, n the number of electrons involved (2 in reaction 1), F the Faraday constant and t is the duration of the corrosion period. Using a density for the material corroding and a measurement of the area of the surface, this mass loss can then be converted into a rate of penetration into the surface. Due to the complications and uncertainties introduced by the presence of grain boundaries and macroscale fractures the measurement of the surface area of UO_2, and especially spent fuel specimens, is fraught with difficulties. These problems in accurately measuring surface areas have been addressed in detail a number of times [12–14].

The two half reactions, (1) and (2) will be influenced by a range of properties of the fuel and its environment. A major feature of the fuel corrosion reaction is the evolution in surface composition with potential, Fig. 8. This relationship between surface composition and potential was determined by X-ray photoelectron spectroscopy (XPS) on electrochemically or naturally corroded [15–18] UO_2 specimens. For electrochemical conditions the potential represents the applied potential while, at the fuel surface, for natural corrosion conditions it is the corrosion potential (E_{CORR}) of the fuel. The various stages of oxidation can be appreciated by the variation in electrochemical current with potential seen in a cyclic voltammetric experiment as illustrated in Fig. 9.

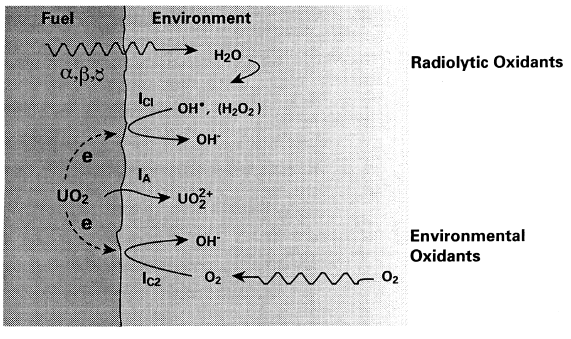

Fig. 7. Schematic diagram illustrating the electrochemical coupling of the anodic fuel dissolution reaction to the cathodic oxidant reduction reaction. Oxidants may be supplied from the external environment or by the radiolysis of water. The anodic current (the fuel dissolution rate) will be equal to the sum of the individual oxidant reduction currents; i.e., $I_A = |I_{C1} + I_{C2}| = I_{CORR}$.

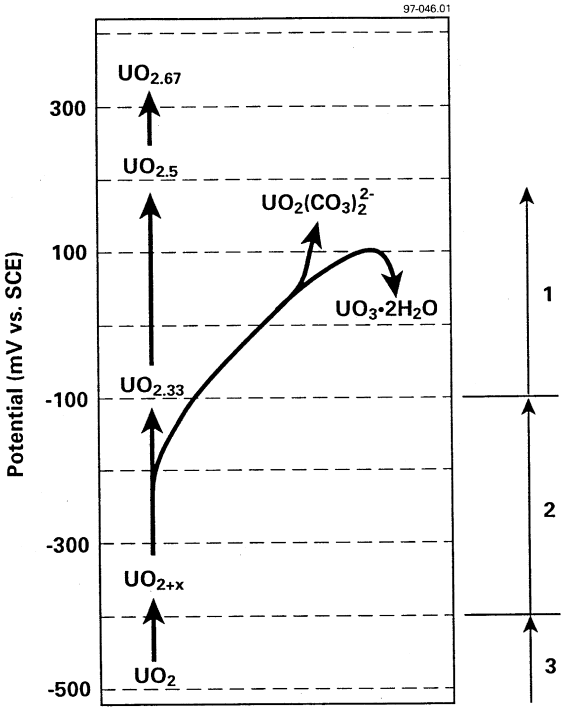

Fig. 8. Chemistry/electrochemistry of UO_2 oxidation and dissolution (corrosion) as a function of electrochemically applied potential or corrosion potential.

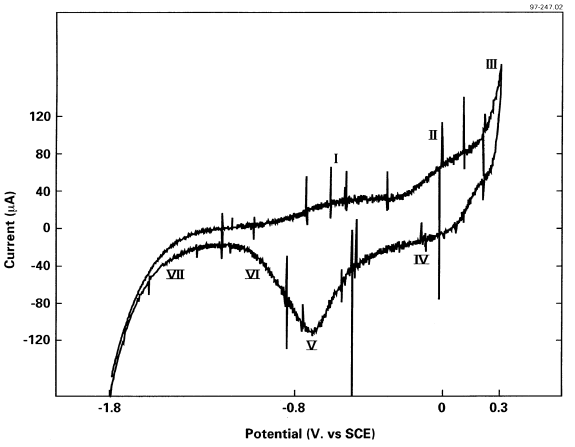

Fig. 9. Cyclic voltammogram recorded on a rotating UO_2 disc electrode at a scan rate of 10 mV s^{-1} and a disc rotation rate of 16.7 Hz using IR compensation in 0.1 mol l^{-1} $NaClO_4$ (pH = 9.5). The Roman numerals indicate the various stages of oxidation (described in the text) or reduction (described in [19]).

Peak (or shoulder) I in Fig. 9 occurs over the potential range −0.8 to −0.4 V (vs SCE). At these low potentials, oxidation should not be thermodynamically possible. This oxidation process is reversible, 100% of the charge being recoverable when the potential scan is reversed for $E \leqslant -0.4$ V. This is consistent with photothermal deflection spectroscopic (PDS) measurements which show no laser beam deflection indicating a change in refractive index of the solution adjacent to the electrode surface indicative of dissolution [20] and with photocurrent spectroscopic (PCS) measurements which show no loss of photocurrent signal due to the destruction of the space charge layer in the oxide which would accompany the irreversible oxidation of the p-type UO_2 surface [4]. Since only small amounts of charge are involved, oxidation appears to be confined to submonolayer areas of the surface. It has been proposed that oxidation occurs at grain boundaries where enhanced hyperstoichiometry could exist due to an inefficient reductive sintering process during fabrication.

Peak II is attributed to the oxidation of the UO_2 electrode matrix involving the incorporation of O^{2-} ions at the interstitial sites in the fluorite lattice until a stoichiometry close to $UO_{2.33}$ is achieved. The oxidation becomes irreversible beyond ∼−0.4 V as indicated by the loss of a photocurrent signal after scanning this potential region [4], and the detection of dissolution by PDS at potentials as low as ∼−0.3 V [20].

As the potential is increased beyond −0.4 V, the thickness of this oxidized surface layer increases under both electrochemical and natural corrosion conditions [4]. A surface composition close in stoichiometry to $UO_{2.33}$ to $UO_{2.4}$ is achieved around −100 mV. Beyond this potential, dissolution as UO_2^{2+} begins to dominate over the thickening of the $UO_{2.33}$ surface oxide layer, which reaches a steady-state thickness of 5–10 nm, region III in Fig. 9. [1] At higher temperatures, (100°C to 200°C) this layer reaches a constant composition but continues to increase in thickness with time. The depth of oxidation also increases with temperature [21,22].

Before proceeding to discuss the chemistry/electrochemistry under steady-state corrosion conditions, it is worth discussing the claim that oxidation occurs preferentially at hyperstoichiometric sites, most probably in grain boundaries. PDS and voltammetric experiments performed on single crystals, in which grain boundaries are absent, showed no significant oxidation current in region I, extremely small currents in region II, and no dissolution (Rudnicki and Russo, private communication, 1996). Voltammetric experiments with specially prepared hyperstoichiometric UO_{2+x} specimens exhibit a very large enhancement of the oxidation current in both regions I and II (Fig. 9) [23]. The rate and depth of oxidation increased with the degree of hyperstoichiometry.

Clearly, the presence of hyperstoichiometric UO_{2+x} in grain boundaries would enhance the reactivity of these sites. Preferential oxidation at these sites is likely to be attenuated by the slight shrinkage in unit cell parameters as UO_2 oxidation occurs. This shrinkage has been noted to weaken the grain boundary regions in spent fuel, introducing a friable nature to the fuel pellets [24,25]. This would be a particularly important process if it occurred during the corrosion of spent fuel since many fission products reside at the grain boundaries.

Once dissolution commences there is the possibility of precipitating U^{VI}-containing phases on the fuel surface leading to some degree of blockage of the corrosion process. Whether or not such phases form will depend on the ratio of the surface area of the fuel to the volume of available solution, the solubility of the UO_2^{2+} in the solution, and the local solution transport regime. Fig. 10 shows electrochemically determined dissolution currents as a function of applied potential in neutral non-complexing solution. These results have been discussed in detail elsewhere [26,27] and only their relevance to the present discussion will be included here.

In region A (⩽300 mV), the fuel is undergoing alteration and close to 100% of the U^{VI} produced accumulates on the fuel surface, as UO_3xH_2O, blocking dissolution. As a consequence, the current, which is the rate of the alteration process under electrochemical conditions, decreases continuously with time and

[1] The reduction processes shown on the reverse potential scan in Fig. 9 are not of immediate importance to this discussion. Their assignment and discussion are given in Luht [19].

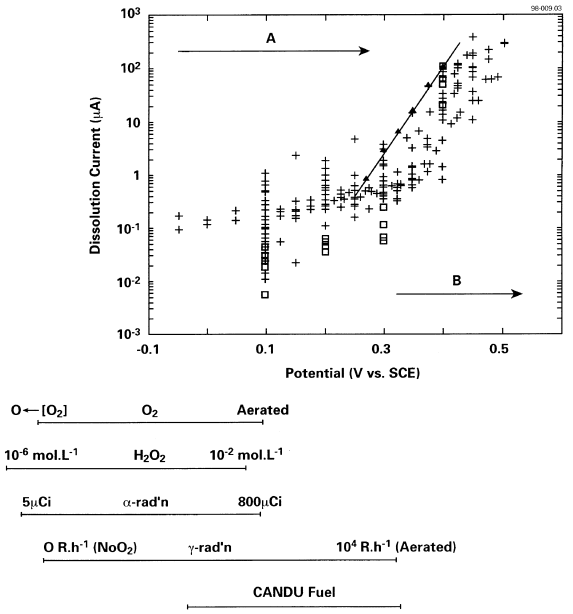

Fig. 10. Electrochemically determined UO_2 dissolution currents as a function of applied potential recorded on a number of different UO_2 rotating disc specimens in 0.1 mol l^{-1} $NaClO_4$ (pH = 9.5) at 16.7 Hz. In region A, the currents are non-steady-state values; in region B, currents are steady-state values [26]. The line connects the data points used in the procedure shown in Fig. 18 to determine UO_2 corrosion rates. The columns of points plotted at 100 and 200 mV are recorded at different times to illustrate the non-steady-state nature of the currents in this region. The large values correspond to short experiments (30 min), the smaller values (□) to long experiments (26 h). The ranges of E_{CORR} values measured in O_2, H_2O_2 solutions, in the presence of γ/α radiation, or on used fuel electrodes, are shown by bars in the figure [27].

steady-state is not achieved. This accumulation of corrosion product is general across the whole of the exposed dissolving surface [19], indicating that general solution saturation occurred under these conditions. In region B ($E > 300$ mV), steady-state dissolution currents were obtained and are logarithmically dependent on potential; i.e. Tafel behaviour was obtained. The reason for this switch in behaviour is that, at these very positive potentials, the rate of anodic dissolution of $UO_{2.33}$

$$UO_{2.33} + 0.33\ H_2O \rightarrow UO_2^{2+} + 0.66\ OH^- + 1.34e^- \quad (4)$$

is sufficiently rapid that extensive hydrolysis to produce local acidity occurs at occluded dissolution sites; i.e.

$$xUO_2^{2+} + yH_2O \rightarrow (UO_2)_x(OH)_y^{(2x-y)+} + yH^+. \quad (5)$$

The pH is suppressed to <5, leading to dissolution of even the $UO_{2.33}$ layer [28] and, hence, a further acceleration in dissolution rate. Also, at these low values of pH the solubility of UO_2^{2+} is increased (Fig. 3), thereby preventing its precipitation and the blockage of the fuel dissolution process. Under these conditions severe etching of the fuel surface, penetration of grain boundaries, and the formation of pits are observed [19]. Similar surface etching, grain boundary penetration and formation of pits were observed by Bottomley et al. [29] at very positive potentials in 3% Na_2CO_3 solutions.

3.1.2. Influence of pH

Attempts to determine the influence of pH on the mechanism of fuel corrosion have been undertaken by a number of authors [28,30,31]. XPS analyses showed that for pH ⩽ 5, the $UO_{2.33}$ layer, which grows as a precursor to dissolution in neutral to alkaline solutions, is not observed. This leads to an increase in dissolution rate (r) with pH, Fig. 11, and a fitted rate equation of the form

$$r = 3.5(\pm 0.8) \times 10^{-8}[H^+]^{0.37\pm0.01}[O_2]^{0.31\pm0.02} \quad (6)$$

for the pH range, $3 < pH < 6.7$, where r has the units of mol m^{-2} s^{-1}. The absence of an oxidized surface layer indicated that the proton-mediated transfer of U^{VI} species to solution was too fast to allow the incorporation of O^{2-} species into the UO_2 lattice [31].

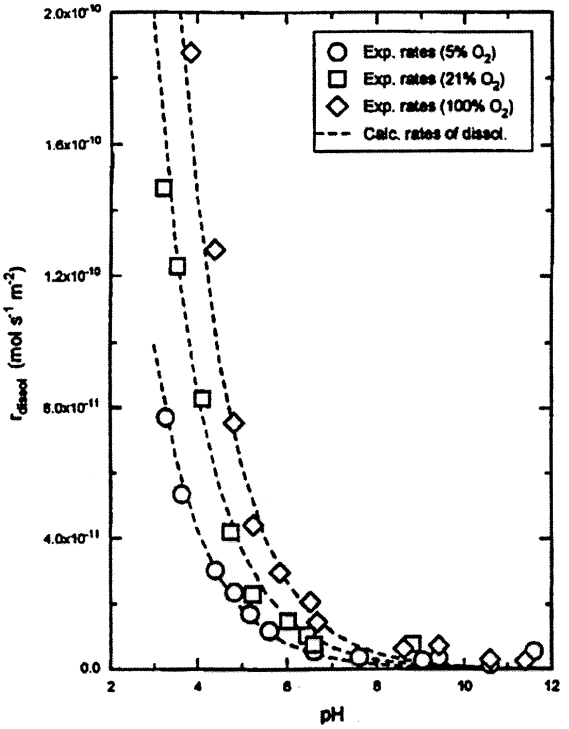

Fig. 11. UO_2 corrosion rates as a function of pH and oxygen concentration measured by the single-pass flow-through technique in 0.01 mol l^{-1} $NaClO_4$ [31]; (○) 5% O_2 in the gas purge; (□) 21% O_2; (◊) 100% O_2.

The partial reaction order with respect to $[H^+]$ was interpreted as an indication that complexed surface species were involved in the dissolution step. This is consistent with impedance spectroscopy data which clearly showed a response attributable to the presence of surface intermediates in the dissolution process in acidic solutions (Shoesmith, unpublished data). Based on steady-state electrochemical dissolution currents, Nicol and Needes [30] showed that both anions (in their case SO_4^{2-}) and cations affected dissolution. While the chemical identity of these intermediates remains obscure, and their nature is likely to change with solution composition, their presence appears well documented. The fractional dependence of dissolution rate on $[O_2]$ (Eq. (6)) has no ready explanation, but the reaction order value of 0.3 was less than the value of 0.7 claimed for $MgCl_2$ solutions with a pH = 4.5 [32], an environment in which XPS also showed the absence of an intermediary $UO_{2.33}$ layer [17]. In electrochemical terms, a fractional reaction order is an indication that no clear anodic or cathodic rate controlling step can be assigned, a concept not at odds with the qualitative argument offered by Torrero et al. [31], that O_2 and H^+ compete for key surface sites.

3.1.3. Influence of carbonate

Of all the potential groundwater species, the one most likely to accelerate UO_2 dissolution under the natural pH conditions expected in a repository is carbonate, a strong complexing agent for the UO_2^{2+} ion [33],

$$UO_2^{2+} + 2CO_3^{2-} \iff UO_2CO_3(aq) \quad (7a)$$

$$\log K_1 = 9.5 \pm 0.4 \quad (7b)$$

$$UO_2^{2+} + 2CO_3^{2-} \iff UO_2(CO_3)_2^{2-} \quad (7c)$$

$$\log \beta_2 = 16.6 \pm 0.3 \quad (7d)$$

$$UO_2^{2+} + 3CO_3^{2-} \iff UO_2(CO_3)_3^{4-} \quad (7e)$$

$$\log \beta_3 = 21.6 \pm 0.6 \quad (7f)$$

On the basis of electrochemical data it appeared that carbonate had no influence on the initial oxidation of UO_2 to $UO_{2.33}$ [34,35]. However, XPS analyses of UO_2 surfaces after long (100 day) exposures to carbonate solutions showed a stoichiometry of $UO_{2.05}$ [18], good evidence that dissolution was not mediated by a significant $UO_{2.33}$ layer, at least for carbonate concentrations of $\sim 10^{-2}$ mol l^{-1}. As for acidic solutions, de Pablo et al. [18] interpreted this as an indication that the transfer of oxidized U species to solution, as UO_2^{2+}, was sufficiently accelerated by complexation with carbonate that the incorporation of O^{2-} into a stable oxidized surface layer did not occur. Such a conclusion is consistent with the PDS and photocurrent observations which show dissolution can occur as soon as the irreversible oxidation of the surface commences. As demonstrated by de Pablo et al. [18] and Torrero et al. [31], whether or not an oxidized layer forms is subsequently determined by the relative rates of the incorporation of O^{2-} to produce $UO_{2.33}$ and the ion transfer of UO_2^{2+} to solution.

Fig. 12 shows anodic dissolution currents measured at different carbonate concentrations. Line 1 is the fit to the triangular points in Fig. 10 and the dashed line 2 is of similar slope but shifted up by two orders of magnitude in current to illustrate the major influence on dissolution currents exerted by carbonate. That both the slopes of these log current–potential relationships and the reaction orders with respect to carbonate concentration change with both potential and carbonate concentrations is a good indication that the mechanistic influence of carbonate is complex. The presence of surface adsorbed intermediates has been clearly demonstrated by impedance spectroscopy experiments [4] for concentrations $>10^{-2}$ mol l^{-1}. Originally these intermediates were thought to be formed on the surface of an underlying $UO_{2.33}$ film but the recent XPS evidence of de Pablo et al. [18] indicates this is not so. The most appropriate mechanism for dissolution involving uranyl carbonate intermediates appears to be

$$\begin{aligned} UO_2 + HCO_3^- &\rightarrow (UO_2HCO_3)_{ads} + e \\ (UO_2HCO_3)_{ads} + OH^- &\rightarrow (UO_2CO_3)_{ads} + H_2O + e \\ (UO_2CO_3)_{ads} + HCO_3^- &\rightarrow UO_2(CO_3)_2^{2-} + H^+ \\ UO_2(CO_3)_2^{2-} + HCO_3^- &\rightarrow UO_2(CO_3)_3^{4-} + H^+. \end{aligned} \quad (8)$$

More generally, the influence of carbonate can be categorized as a function of concentration according to the schematics shown in Fig. 13:

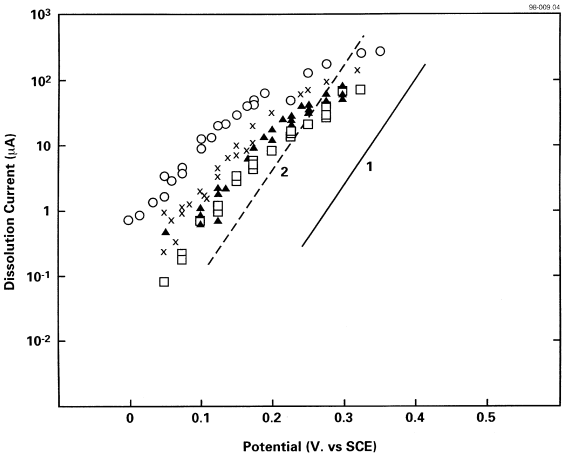

Fig. 12. Electrochemically determined UO_2 dissolution currents as a function of applied potential recorded on UO_2 rotating disc electrodes ($\omega = 16.7$ Hz) in 0.1 mol l^{-1} $NaClO_4$ (pH = 9.5) containing various concentrations of carbonate: (□) 0.005 mol l^{-1}; (▲) 0.01 mol l^{-1}; (×) 0.05 mol l^{-1}; (○) 0.1 mol l^{-1}. Line 1 is the line from Fig. 10. Line 2 is a line of identical slope to line 1 for currents increased by two orders of magnitude [27].

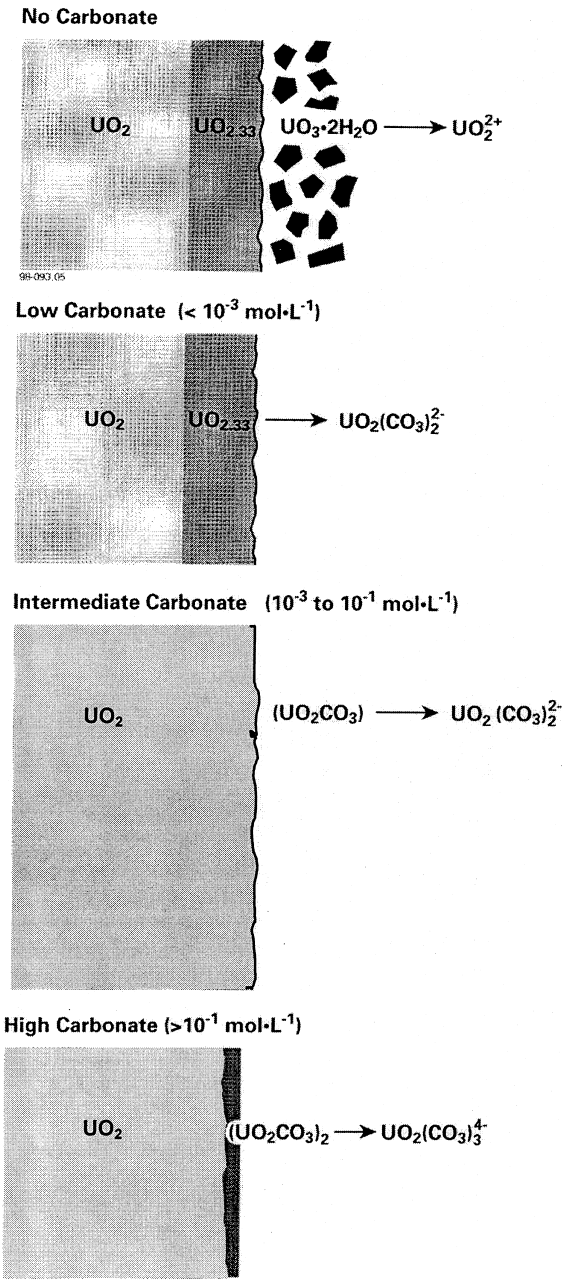

Fig. 13. Schematic diagrams illustrating the influence of carbonate on UO_2 dissolution as the concentration changes.

1. in the absence of carbonate, corrosion product deposits can accumulate and suppress the dissolution rate (line 1 in Fig. 12);
2. at low concentrations ($\leqslant 10^{-3}$ mol l^{-1}) the predominant influence of carbonate seems to be the thermodynamic ability to increase UO_2^{2+} solubility and, hence, to prevent the deposition of corrosion product deposits (line 2, Fig. 12);
3. for intermediate concentrations (10^{-3} to 10^{-1} mol l^{-1}), HCO_3^-/CO_3^{2-} is kinetically involved, via the formation of surface intermediates, in the dissolution process;
4. for high concentrations, the presence on the surface of a phase such as UO_2CO_3 begins to limit the rate of dissolution and the reaction becomes much less dependent on carbonate concentration.

3.1.4. Influence of other potential groundwater species

The other critical groundwater species are those which will retard dissolution by enhancing the formation of corrosion product deposits with extremely low solubilities. Of the potential groundwater species the ones most likely to lead to the formation of insoluble deposits are Ca and Si.

Electrochemical experiments followed by XPS analyses show that the incorporation of these two species into corrosion product films at oxidizing potentials (i.e. in region A of Fig. 10) leads to the rapid suppression of dissolution currents. Fig. 14 shows values of the charge associated with the subsequent electrochemical stripping of these corrosion product deposits. This charge is an effective measure of the thickness of the corrosion product deposit assuming it to be evenly distributed across the surface. At all potentials in region A ($\leqslant$0.4 V in this case), the films formed in Standard Canadian Shield Saline Solution (containing 3.7×10^{-1} mol l^{-1} of Ca^{2+} and 5.4×10^{-4} mol l^{-1} of Si^{4+}) are thinner (meaning less alteration has occurred) than those formed in simple electrolytes not containing Ca^{2+} and Si^{4+}, and, although not apparent from this figure, more able to protect the underlying UO_2 from dissolution [19]. They also continue to thicken at very positive potentials (indicative of extreme oxidizing conditions) thereby

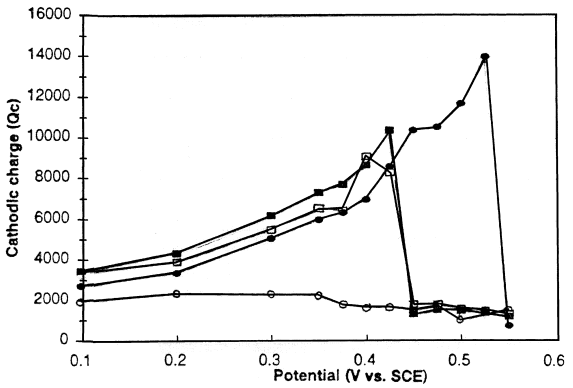

Fig. 14. Film thicknesses (expressed in coulombs) for corrosion product films electrochemically grown on UO_2 electrodes for 90 min at different applied potentials in different neutral electrolytes: (■) 0.1 mol l^{-1} $NaClO_4$; (□) 0.97 mol l^{-1} NaCl; (●) SCSSS, a Ca^{2+}, Si^{4+} containing simulated groundwater (see text); (○) SCSSS + 10^{-2} mol l^{-1} HCO_3^- [19].

preventing the transition to region B ($\geqslant$0.4 V) and the development of aggressive local acidic conditions, and the dominance of dissolution over the accumulation of corrosion product deposits. The transition to region B occurs for $E \geqslant 0.42$ V and is indicated by the sudden drop in film thickness (cathodic charge) in Fig. 14. The very low values of cathodic charge when carbonate is present show that the ability of carbonate to promote dissolution counterbalances any tendency for Ca and Si to promote the development of thick corrosion product layers.

Based on the above discussion, we can define the behaviour to be expected on the surface of fuel as a function of potential, whether this potential be applied electrochemically, as was the case in most of the experiments described, or achieved naturally by exposure of the fuel to an environment of known redox condition.

1. -800 mV $\leqslant E \leqslant -400$ mV; oxidation of submonolayer quantities of surface material, possibly concentrated in grain boundaries.
2. -400 mV $\leqslant E \leqslant -100$ mV; irreversible oxidation of the UO_2 lattice to UO_{2+x} occurs with both x and the depth of oxidation increasing with potential to a limiting composition of $\sim UO_{2.33}/UO_{2.4}$ at -100 mV. Dissolution as UO_2^{2+} begins at ~ -300 mV (in neutral to slightly alkaline solution). Both oxidation and dissolution appear to start preferentially in grain boundaries if these sites are hyperstoichiometric.
3. -100 mV $\leqslant E \leqslant +300$ mV. Oxidation, dissolution and the accumulation of corrosion product deposits occur. The balance between dissolution and the formation of corrosion product deposits varies with pH, solution composition and the local transport regime.
   (a) In non-complexing neutral solutions, corrosion product deposits accumulate and block fuel dissolution.
   (b) For pH $\leqslant$ 5, corrosion product deposition no longer occurs, oxidation to $UO_{2.33}$ is prevented, and, hence dissolution accelerated.
   (c) In neutral solutions containing sufficient HCO_3^-/CO_3^{2-} ($\geqslant 10^{-3}$ mol l^{-1}), $UO_{2.33}$ does not form, corrosion product deposits are avoided, and dissolution accelerated.
   (d) In Ca/Si-containing groundwaters the formation of protective corrosion product deposits is reinforced.
4. $E > +300$ mV; rapid dissolution leads to the development of local acidity causing grain boundary etching and pitting. The dissolution rate increases since corrosion product deposition is prevented.

3.2. Corrosion behaviour of UO_2

The corrosion behaviour of UO_2 in near neutral to alkaline solutions, the environment expected to prevail in most waste repositories, [2] can be summarized in terms of the schematic of E_{CORR} as a function of time shown in Fig. 15. The reaction sequence shown has been demonstrated for open-circuit corrosion conditions by electrochemical and XPS experiments and is identical to the sequence determined electrochemically and summarized above [15,18,36]. This relationship between E_{CORR} and surface composition is clearly shown in Figs. 16 and 17, which show the cathodic film charge (directly proportional to film composition and thickness) [3] and the stoichoimetry of the UO_2 surface as a function of E_{CORR}. These values were determined after exposure to gamma irradiated solutions in which each experiment was stopped at a different value of E_{CORR}, irrespective of whether this value was achieved quickly at high dose rates or slowly at low dose rates [36]. The growth and change in composition of the film (up to $\sim UO_{2.33}/UO_{2.4}$) over the potential range -400 mV to ~ 0 mV are clearly shown. For higher values of E_{CORR} the accumulation of a predominantly U^{VI} deposit (i.e., high values of the U^{VI}/U^{IV} ratio) occurs once a steady-state value of E_{CORR} was achieved.

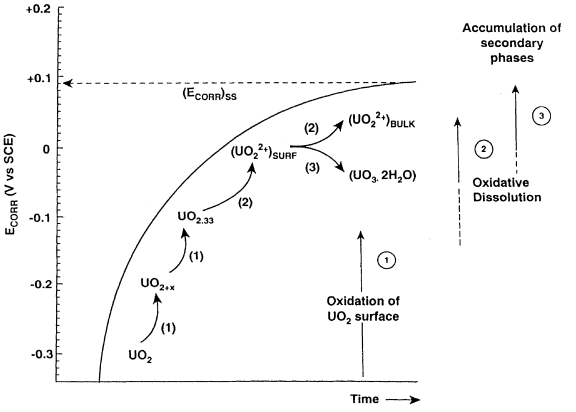

Fig. 15. Schematic diagram indicating the stages of oxidation observed on the surface of UO_2 fuel as the corrosion potential (E_{CORR}) changes with time and approaches the steady-state value of $(E_{CORR})_{SS}$.

This form of E_{CORR} – time curve (Fig. 15) has been obtained in a wide range of environments including aerated solutions [15,28], H_2O_2 solutions [37], gamma and alpha radiolytically decomposed solutions [36,38] and on spent fuel [39] and SIMFUEL electrodes [40]. The rate at which the steady-state E_{CORR} value ($(E_{CORR})_{SS}$) is achieved is a measure of the kinetics of the

[2] Repositories with Mg-containing brines, when the pH could be <5, may be the only exception.

[3] A charge, $Q_c \sim 8$ mC, on the electrode used would be equivalent to a surface film thickness of 4 nm to 8 nm, depending on the film composition assumed.

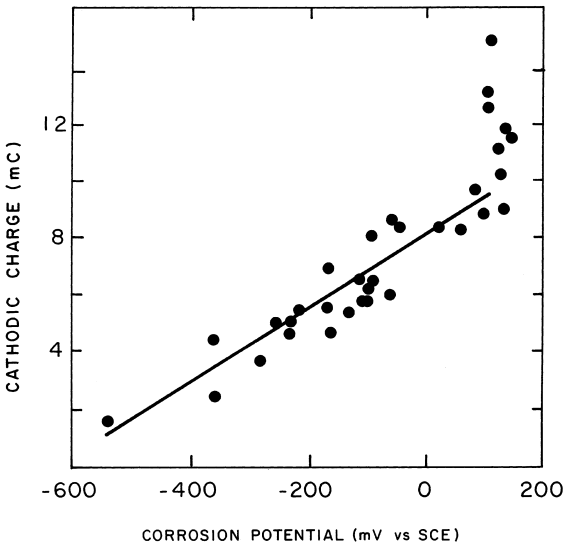

Fig. 16. Cathodic charge measured by cathodic-stripping voltammetry as a function of the corrosion potential (E_{CORR}) achieved under natural corrosion conditions in 0.1 mol l^{-1} $NaClO_4$ (pH = 9.5) gamma-irradiated at various absorbed dose rates for various times [36].

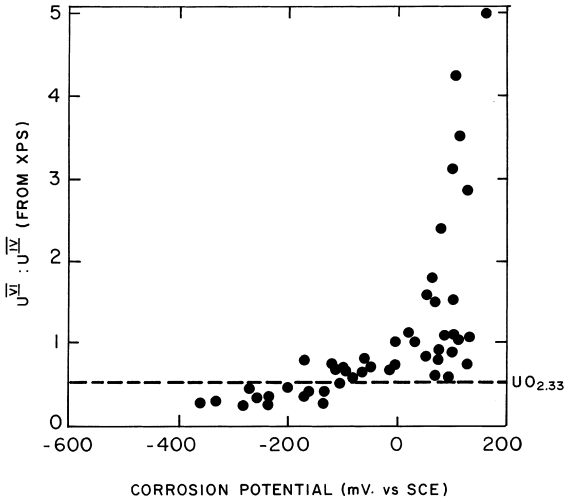

Fig. 17. $U^{VI} : U^{IV}$ ratio in the surface of a UO_2 specimen after corrosion in 0.1 mol l^{-1} $NaClO_4$ (pH = 9.5) gamma-irradiated at various absorbed dose rates for various times [36].

fuel oxidation reaction $UO_2 \rightarrow UO_{2.33}/UO_{2.4}$, and the value of $(E_{CORR})_{SS}$ is an indication of the relative balance of the kinetics of the anodic and cathodic half reactions (reactions (1) and (2)). Values of $(E_{CORR})_{SS}$ can be used with appropriate values of electrochemically determined steady-state dissolution currents (as plotted in Figs. 10 and 12) to determine fuel dissolution rates. The procedure, the well-known Tafel extrapolation, is illustrated in Fig. 18.

One point worth noting at this juncture is that the electrochemically determined reaction order for a particular reactant (e.g. carbonate from Fig. 12) will not necessarily translate, by an extrapolation as shown in Fig. 18, to an identical reaction order for the overall corrosion process. This is because the log current–potential plot represents the kinetics of the particular half reaction (anodic or cathodic) while $(E_{CORR})_{SS}$ is determined by the relative kinetics of both half reactions. This issue has been dealt with in more detail elsewhere [27].

4. Mechanism of reduction of various oxidants

The rate of fuel corrosion will be dictated predominantly by the nature and concentration of environmental and radiolytic oxidants. The primary oxidants will be O_2, supplied to the repository by transport from the external environment, and the products of the alpha, beta and gamma radiolysis of water contacting the fuel. A significant amount of effort has gone into the determination of the mechanism of reaction of these various oxidants with UO_2 fuel.

4.1. Reduction of O_2

The cathodic reduction of O_2 is a notoriously slow reaction [41], due to the need to break the strong O–O bond, and on oxide surfaces inevitably involves catalysis by mixed oxidation states available on the surface of the oxide [42]. Based on the theory of Presnov and Trunov [43], developed to explain the reduction of O_2 on transition metal oxides with p-type semiconductivity, these mixed oxidation states are donor–acceptor sites. These sites are available on the surface of the fuel where U atoms are present as U(VI) or U(V) above U(V) or U(IV).

The process is illustrated schematically in Fig. 19(A). The oxidized U atom in the surface accepts an electron from the bulk of the oxide and subsequently donates it to an O_2 atom adsorbed under Langmuir conditions. The first-order dependence of the overall reduction reaction on $[O_2]$ and large Tafel slopes ($dE/d\log i$) clearly indicate that the first electron transfer step is rate-determining. Subsequent reduction of the adsorbed superoxide ion to hydroxide ion then proceeds rapidly via a series route involving single electron and proton transfer steps.

The large measured Tafel slope (180–240 mV), and the variation of this slope with potential, suggest a dependence of O_2 reduction kinetics on the surface composition of the fuel and its variation with potential [44]. Consequently, we would expect the kinetics of O_2

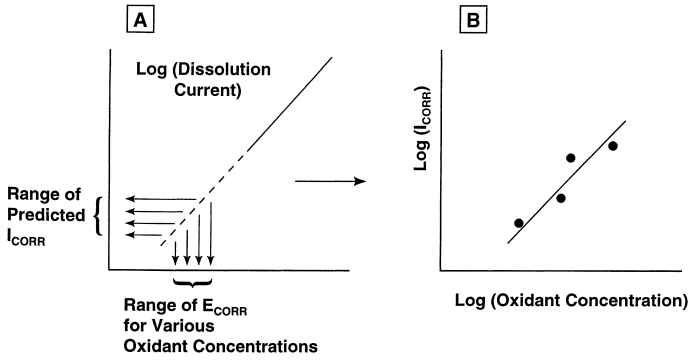

Fig. 18. Illustration of the procedure used to obtain corrosion currents (I_{CORR}), and hence corrosion rates, from electrochemically measured dissolution currents and corrosion potential (E_{CORR}) measurements: (A) Tafel relationship relating anodic dissolution currents to applied electrochemical potentials. (B) The dashed section of the line indicates the extrapolation of measured currents to the measured corrosion potential (E_{CORR}) to obtain the values of corrosion current plotted as a function of oxidant concentration.

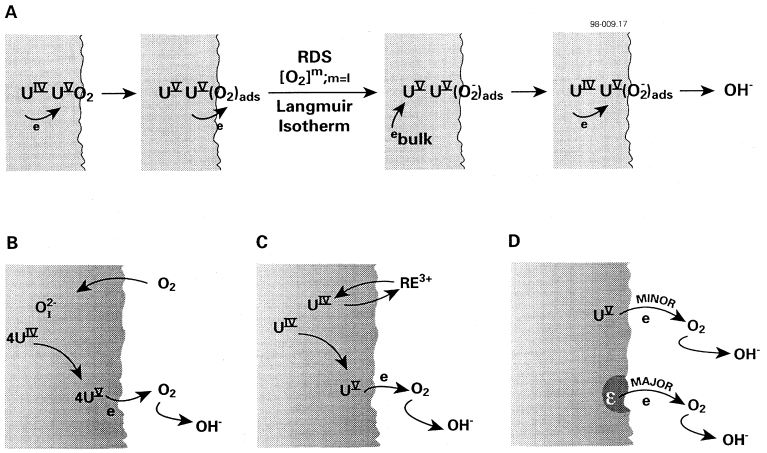

Fig. 19. Schematic diagrams illustrating the influence of various factors on a O_2 reduction on a UO_2 surface: (A) mechanism of reduction at donor–acceptor sites; (B) effect of corrosion on the number density of donor–acceptor sites; (C) effect of rare earth doping on the number density of donor–acceptor sites; (D) catalytic effect of noble metal particles (ε phase).

reduction to change with redox conditions since the composition of the fuel surface (i.e., the number of available U^{IV}/U^{V} or U^{V}/U^{VI} sites) varies from UO_2 to $UO_{2.33}$ as the oxidant concentration varies [36]. This is confirmed by the observed increase in O_2 reduction current as the number of these sites is increased by oxidation the fuel surface after natural corrosion in aerated solutions [41] as shown in Fig. 20. This effect is illustrated schematically in Fig. 19(B). More extensive oxidation of the surface leading to the accumulation of deposited corrosion products causes a suppression of the O_2 reduction current suggesting blockage of the donor–acceptor sites [41].

Enhanced non-stoichiometry of the fuel, due to either incomplete sintering during fabrication or changes induced by in-reactor exposure, can also change the kinetics of O_2 reduction [23]. If this non-stochiometry is inhomogeneously distributed, i.e., located within grain boundaries or present as derivative phases throughout the structure (e.g. U_4O_{9-y}), then the rate of O_2 reduction will vary from site to site [39]. This is particularly noticeable under oxidizing conditions since the rate of fuel oxidation (and, hence, the number of donor–acceptor sites) increases rapidly with an increase in degree of non-stoichometry [23].

Two effects on in-reactor fission are expected to influence the kinetics of O_2 reduction: (i) the formation of rare earth (RE) elements (e.g. Y, Nd in the 3+ oxidation state) in solid solution with U (predominantly in the 4+ state); and (ii) the formation of noble-metal particles (Ru, Mo, Rh, Pd) predominantly present as segregants on the grain boundaries. These particles, known as the

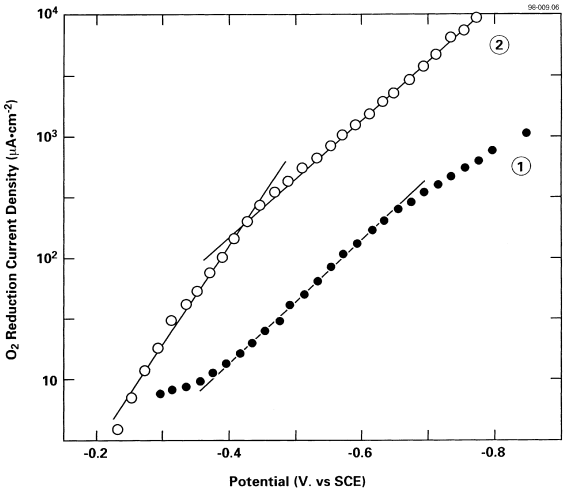

Fig. 20. Transport- and IR-compensated O_2 reduction currents recorded on a UO_2 rotating disc electrode as a function of potential in aerated 0.1 mol l^{-1} $NaClO_4$ (pH = 9.5). The electrode was electrochemically reduced in Ar-purged solution before the experiment: (1) data recorded from the most negative to most positive potential; (2) data recorded from the most positive to most negative potential after corrosion in the aerated solution until $(E_{CORR})_{SS}$ was achieved (~4) days) [41].

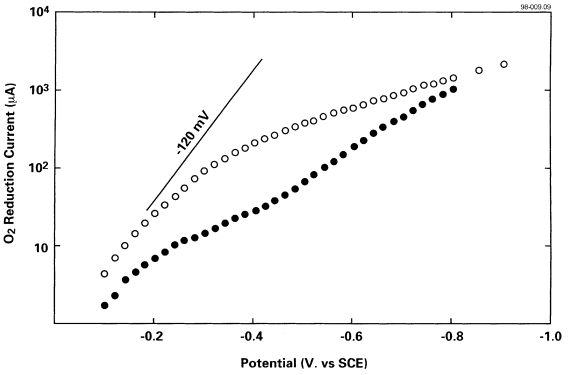

Fig. 21. Transport- and IR-compensated O_2 reduction currents as a function of applied potential recorded on a SIMFUEL (3 at.% simulated burnup) rotating disc electrode in aerated 0.1 mol l^{-1} $NaClO_4$ (pH = 9.5): (○) after cathodic reduction at −2 V; (●) after corrosion in aerated solution to an E_{CORR} value of 134 mV (vs. SCE) [27].

ε-phase, are present as a hexagonal close-packed alloy with an average composition (in at.%) of Ru-47/Mo-28/Pd-22/Rh-3. The introduction of RE^{3+} species leads to the conversion of an equivalent amount of U^{4+} to U^{5+} (i.e., the creation of donor–acceptor sites), as shown schematically in Fig. 19(C).

The influence of these effects on the kinetics of O_2 reduction has been studied using a range of SIMFUEL specimens in which the chemical effects of fission products were replicated by incorporation of 11 stable elements (Ba, Ce, La, Mo, Sr, Y, Zr, Rh, Pd, Ru and Nd) in suitable proportions to simulate various burnup levels [23]. The results of these studies show that, while the influence of rare earth doping of the fuel has only a marginal effect on the kinetics of O_2 reduction, the presence of the noble metal segregants has a very major effect, Fig. 19(D). This enhancement suggests that the noble-metal particles have similar electrocatalytic properties to the metals incorporated in the alloy. The elements Pd, Rh and Ru all possess greater reactivity than UO_2 for O_2 reduction by factors ranging from $<10^2$ (Ru) to $>10^4$ (Pd).

Since corrosion of fuel will proceed most rapidly for the most oxidizing conditions, the critical surface state is that present under these conditions. Consequently, the current–potential relationships recorded on the naturally corroded surfaces are the most relevant. However, while natural corrosion leads to the catalysis of O_2 reduction on UO_2 it suppresses this reaction on SIMFUEL surfaces, Fig. 21, the currents being approximately the same on both oxidized surfaces. This suggests that the ability of the noble metal ε-particles to catalyze O_2 reduction is lost by the formation of a passive film. An attempt to represent these conflicting effects on UO_2 and the ε-particles is shown in Fig. 22. Based on these observations, the presence of ε-particles in spent fuel specimens would not be expected to exert any significant influence on their dissolution properties under oxidizing conditions.

Measurements of $(E_{CORR})_{SS}$ as a function of O_2 concentration show a dependence on O_2 concentration which translates, via the extrapolation shown in Fig. 18, to a prediction that the fuel corrosion rate in neutral non-complexing solutions will be close to first order with respect to O_2 [16].

4.2. Reduction of H_2O_2

There is good evidence to indicate that H_2O_2 reduction is a significantly faster reaction on UO_2 than O_2 reduction. Thus, measurements of the rate of change of E_{CORR} in neutral solutions show that the oxidation of UO_2 to $UO_{2.33}$ is ~200 times faster in H_2O_2 than in a solution containing an equal concentration of O_2 [37]. Also, the current for H_2O_2 reduction is one to two orders of magnitude larger than for O_2 reduction at the same applied potential, Fig. 23.

Despite this clear evidence that H_2O_2 reduction is fast and able to drive the oxidation of UO_2 much faster than O_2 reduction, the next step in the overall corrosion process, the oxidative dissolution of $UO_{2.33}$ to soluble UO_2^{2+}, appears to proceed at roughly the same rate irrespective of which oxidant is present. This is based on the observation that $(E_{CORR})_{SS}$ does not vary with H_2O_2 concentration over the range 10^{-4} mol $l^{-1} \leqslant$

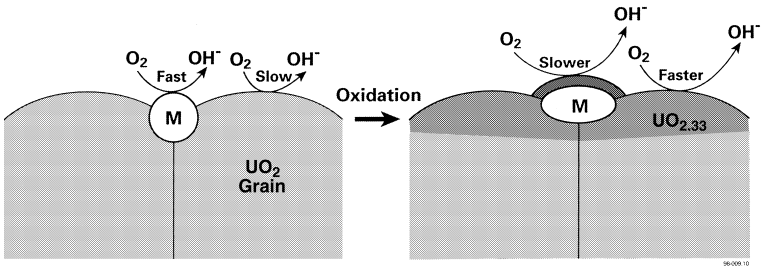

Fig. 22. Schematic diagram showing the effect of surface oxidation on the kinetics of O_2 reduction on UO_2 grains an noble metal particles (ε phase, denoted M).

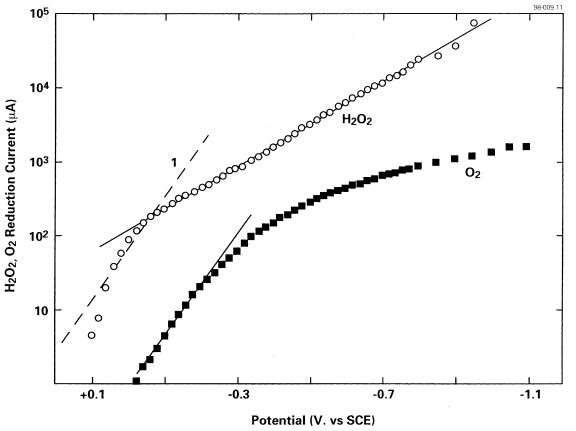

Fig. 23. Transport- and IR-compensated reduction currents recorded on a SIMFUEL rotating disc electrode (3 at.% simulated burnup) in 0.1 mol l^{-1} $NaClO_4$ (pH = 9.5): (○) $[H_2O_2] = 5 \times 10^{-4}$ mol l^{-1}; (■) $[O_2] = 2.7 \times 10^{-4}$ mol l^{-1}. Line 1 is drawn with the same slope as the line drawn to fit the low potential data recorded in O_2-containing solution to illustrate that the same Tafel relationship is not observed in H_2O_2 solution as in O_2 solution [27].

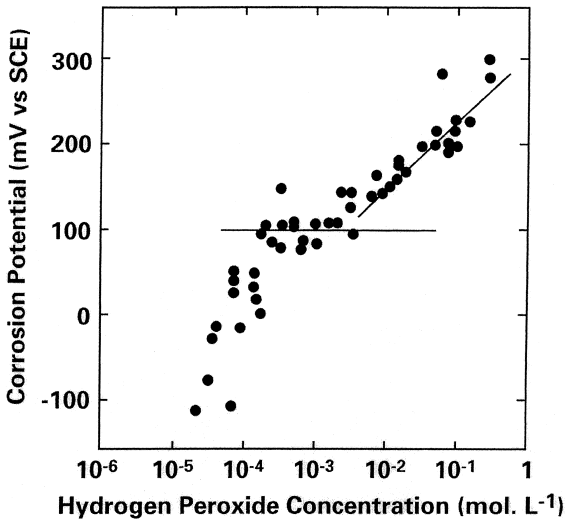

Fig. 24. Steady-state corrosion potential $(E_{CORR})_{SS}$ values measured as a function of H_2O_2 concentration in 0.1 mol l^{-1} $NaClO_4$ (pH = 9.5) [16].

$[H_2O] \leqslant 10^{-2}$ mol l^{-1} [16], Fig. 24. The most probable explanation for these observations is that the reduction of H_2O_2 couples more readily to H_2O_2 oxidation (to yield the decomposition products, H_2O and O_2) than it does to the oxidation of $UO_{2.33}$ to yield UO_2^{2+}. That H_2O_2 decomposition can occur has been demonstrated under corrosion conditions [45] and under electrochemical conditions [46].

According to this scheme, H_2O_2 would be rapidly decomposed on the fuel surface and the corrosion rate subsequently determined by reaction of the fuel with the decomposition product, O_2. Since the local concentration of O_2 at the fuel surface will be regulated by its solubility it is possible that the independence of E_{CORR} on $[H_2O_2]$ is actually attributable to a constant $[O_2]$. An attempt to represent this situation schematically is shown in Fig. 25(A). That such a reaction should occur on a $UO_{2.33}(U_2^{IV}U^{VI}O_7)$ surface is not unexpected since H_2O_2 decomposition is known to be catalysed on oxide surfaces containing mixed oxidation states, as illustrated schematically for UO_{2+x} in Fig. 25(B) [16].

The redox buffering of the fuel surface by hydrogen peroxide is lost under a number of circumstances. For concentrations $> 10^{-2}$ mol l^{-1}, $(E_{CORR})_{SS}$ increases with peroxide concentration suggesting that the fuel corrosion reaction is becoming more important than H_2O_2 decomposition, Fig. 24. The rate of corrosion for this concentration range is predicted to have a first-order dependence on H_2O_2 concentration, consistent with the observations of Gimenez et al. [47]. Again, in agreement with the above observations, they measured the rate to be independent of $[H_2O_2]$ between 10^{-2} and 10^{-3} mol l^{-1}.

Interestingly, this positive shift in $(E_{CORR})_{SS}$ is prevented by the addition of carbonate, and the $(E_{CORR})_{SS}$ remains effectively independent of $[H_2O_2]$ to concentrations up to nearly 1 mol l^{-1} [16]. The accumulation of a corrosion product deposit, indicated by an increase in U(VI) to U(IV) ratio measured by XPS, observed in this

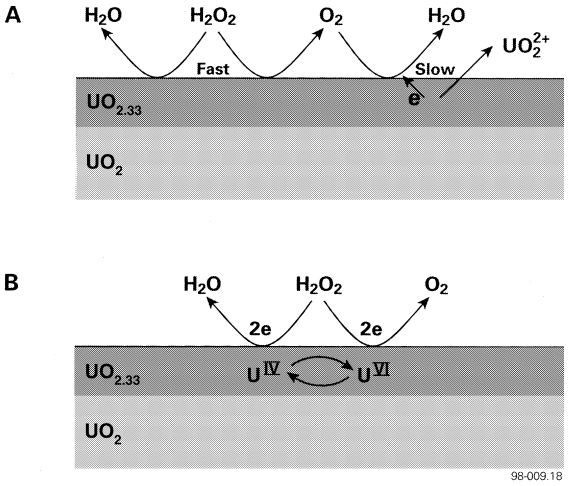

Fig. 25. Schematic diagrams illustrating the behaviour of H_2O_2 at UO_{2+x} surfaces: (A) the relative rates of H_2O_2 decomposition and fuel corrosion by reaction with the decomposition product, O_2; (B) catalysis of H_2O_2 decomposition by the mixed oxidation states present on the surface of UO_2.

concentration range when carbonate is not present, is prevented when it is. Also, when carbonate is present, the accumulation of gas bubbles on the fuel surface confirms that H_2O_2 decomposition is occurring rapidly for $[H_2O_2] > 10^{-2}$ mol l^{-1}. This last observation indicates that, when carbonate is present, the condition of redox buffering of the UO_2 surface persists to very high $[H_2O_2]$. This suggests that, in the absence of carbonate, the accumulation of a corrosion product deposit blocks these surface sites required to catalyze H_2O_2 decomposition, Fig. 25(A). The very positive potentials achieved at high $[H_2O_2]$, Fig. 24, approach those for which local acidic conditions are anticipated, Fig. 10. When carbonate is present, not only would the deposition of corrosion products be prevented, but any tendency for the pH to decrease at the electrode surface would be neutralized.

Some support for this argument that the positive shift in E_{CORR} may be attributable to the development of local acidity comes from the effect of pH on $(E_{CORR})_{SS}$. As the pH is decreased, E_{CORR} becomes much more positive, achieving values of ~ 200 mV for pH ~ 7 and > 400 mV for pH < 2 [16]. In the pH range 4–6.5 Diaz-Arocas et al. [48] observed aggressive attack of UO_2 in H_2O_2 solutions as well as the accumulation of a corrosion product deposit. This deposit was identified as studtite $(UO_4 \cdot 4H_2O_2)$.

4.3. Reduction of radical oxidants produced by the β/γ radiolysis of water

Given that the rate of H_2O_2 reduction (a two electron process) is fast compared to that of O_2 reduction (four electrons), we would anticipate that the reduction of radical species $(OH^{\cdot}, O_2^{-})$ (1 electron), produced by the β/γ-radiolysis of water, would be even more rapid. Corrosion rates as a function of γ-dose rate, predicted using the procedure shown in Fig. 18, demonstrate that this is indeed the case [16]. These results show, Fig. 26, that, for a sufficiently high dose rate, the corrosion rate is a linear function of the square root of dose rate, i.e., approximately proportional to the sum concentration of radiolytic oxidants.

A possible explanation for this first-order dependence is that the reaction of radical oxidants with UO_2 is diffusion-controlled with all the radicals produced within a thin reaction layer directly adjacent to the fuel surface reacting with it, as illustrated schematically in Fig. 27. The thickness of this reaction layer (x) is determined by the diffusion coefficient of the radical (D_r) and its effective lifetime (τ),

$$\bar{x} = (2D_r\tau)^{1/2}, \tag{9}$$

where τ represents the kinetic balance between the rate of radiolytic production of the radical and its rate of consumption by homogeneous reactions in solution. The thickness of this reaction layer will vary with the nature of the species and the dose rate. Thus, for the $OH^{\cdot}$ radical, x varies from ~ 16 to ~ 44 μm for a change in dose rate from 280 to 5 Gy h^{-1} [49]. As indicated in Fig. 27, β is a low-linear energy transfer (LET) form of radiation whose range in aqueous solution will not be substantially greater than the reaction layer thickness.

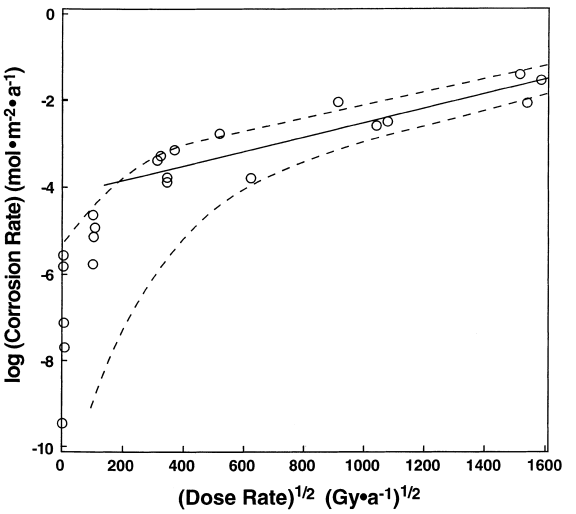

Fig. 26. Corrosion rate of UO_2 as a function of the square root of gamma dose rate in Ar-purged 0.1 mol l^{-1} $NaClO_4$ solution (pH = 9.5) (1R $\equiv 10^{-2}$ Gy). The dashed lines have no fitting significance, but simply bracket the experimental points [16].

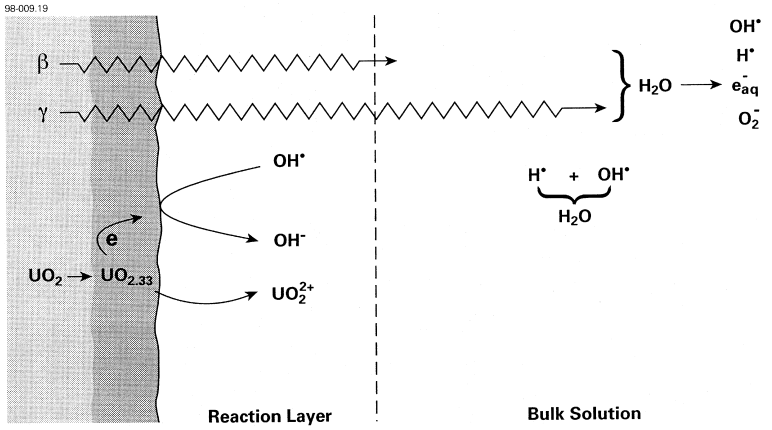

Fig. 27. Schematic diagram illustrating the short-range and long-range influences of β and γ radiation. Only radical oxidants produced within the reaction layer react with UO_2, making β-fields much more efficient than γ-fields.

In a number of experiments at high γ-dose rates ($\sim 10^2$ Gy h^{-1}) $(E_{CORR})_{SS}$ values >300 mV were obtained (Sunder and Shoesmith, unpublished data). The attainment of these positive potentials was accompanied by the accumulation of corrosion product deposits (indicated by XPS measurements) and the generation of a bulk solution pH < 4. It would appear that sufficiently high γ-dose rates can drive E_{CORR} into the potential range (region B in Fig. 10) where local acidic conditions can be sustained in cracks, fissures, grain boundaries and pits created by missing grains.

4.4. Reduction of molecular oxidants produced by the α-radiolysis of water

In contrast to β/γ-radiation, α-radiation is a high LET (linear energy transfer) form of radiation which deposits all its energy in a layer of solution ~25 μm thick adjacent to the fuel surface to produce predominantly the molecular oxidant H_2O_2. A combination of measurements [38,50] and calculations [51] shows that the corrosion behaviour of the fuel exposed to α-radiolytically decomposed water is very similar to that observed in the presence of H_2O_2. For α-source strengths $\geqslant 250$ μ Ci, $(E_{CORR})_{SS}$ becomes independent of source strength, Fig. 28. Calculations of the $[H_2O_2]$ generated at these source strength values in the cell used to make the measurements [51] show they are in the concentration range where $(E_{CORR})_{SS}$ is expected to be independent of $[H_2O_2]$ (Fig. 24). This similarity appears to confirm that the radiolytically produced H_2O_2, and its decomposition to O_2 and H_2O, will be the dominant effects on fuel corrosion in the presence of α-radiation.

In one experiment, using an α-source strength of 686 μ Ci, a non-steady state value of $E_{CORR} > 130$ mV and increasing was obtained [51] suggesting that there is a possibility of local acidification at sufficiently high α-dose rates.

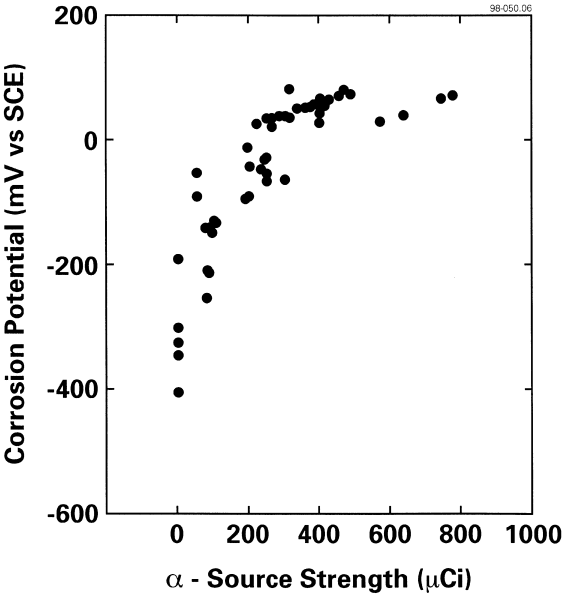

Fig. 28. Steady-state corrosion potential $(E_{CORR})_{SS}$ values measured as a function of α-source strength in 0.1 mol l^{-1} $NaClO_4$ (pH = 9.5) [38].

5. The influence of various parameters on fuel corrosion

A wide range of studies of fuel dissolution have been published. Since potential repository environments range from wet to dry, oxidizing to anoxic, and from dilute to saturated saline groundwater conditions, the results of all these studies are not directly applicable to all repository environments. In many cases specific

parameters deemed important for a particular environment were studied. In this section the influence of various parameters on fuel dissolution will be reviewed with the predominant emphasis being on fuel corrosion as opposed to radionuclide release, since the release rate of the majority of radionuclides will be controlled by the matrix dissolution process. In this regard, this review deals primary with those parameters most likely to influence the release of radionuclides in categories (ii) and (iii) of Section 2.

The following specific areas and parameters are discussed; the intrinsic fuel dissolution rate, fuel preoxidation, pH, O_2 concentration, dependence on carbonate concentration, temperature, radiolysis, a comparison of unirradiated UO_2 and spent fuel (including the influence of spent fuel burnup), the formation of secondary phases as corrosion product deposits.

5.1. Intrinsic corrosion rates

The intrinsic dissolution rates of unirradiated UO_2 and spent fuel have been determined using a single-pass flow-through method described by Gray et al. [13]. The advantage of the single-pass, flow-through technique is that flow rates and specimen size can be controlled so that the UO_2 dissolves under conditions that are far from solution saturation. This minimizes the effect of the precipitation of dissolved corrosion products on the rate. Under such conditions, the steady-state dissolution rates are directly proportional to the effective surface area of the specimen and, subsequently, the dependence of UO_2 dissolution kinematics on parameters such as pH, temperature, O_2, and HCO_3^-/CO_3^{2-} can be evaluated. Besides Gray et al. [13], this experimental technique has been successfully applied by Tait and Luht [14], de Pablo et al. [18,52], Bruno et al. [53], and Steward and Mones [54].

Using carefully prepared UO_2 powders from the same source in three different laboratories (Pacific Northwest National Laboratories (PNL), Lawrence Livermore National Laboratories (LLNL) and Whiteshell Laboratories (WL)), the measured rates were 2.2 ± 0.5 (PNL), 5.5 ± 2.7 (LLNL) and 1.5 ± 0.9 (WL) mg m^{-2} d^{-1}. The predominant source of error was the accurate determination of fuel surface area, a measurement complicated by uncertainty over the extent of solution penetration into grain boundaries [12]. While not a major problem for this comparison of measurements of UO_2 from the same source, this uncertainty is a problem when attempting to compare rates on fuel specimens from different sources.

5.2. Pre-oxidation of fuel

Early waste package failure could lead to the dry oxidation of UO_2. For disposal scenarios in which fuel temperatures are high (i.e. $\gg$100°C), which is the proposed condition for the Yucca Mountain repository, fuel oxidation could be extensive. Oxidation of the fuel to U_3O_8 would lead to break up of the fuel grains and to a substantial increase in volume (by a factor of 1.35). This expansion would place stress on the fuel cladding, which could lead to its unzipping, and to the eventual exposure of a large surface area of fuel to water. Gray and Thomas [55] estimated this increase in fuel surface area to be approximately a factor of 150. The mechanism of this process, including the all important temperature dependence, has been reviewed in detail [3,56]. While potentially a dangerous situation, Siegmann [57] has presented calculations to show the process is avoidable providing waste package containment is assured for only 100–150 years.

A more likely possibility is that waste package and cladding failure will expose the fuel to aerated moist environments and that preoxidation will occur by reaction with aerated steam. Johnson and Taylor [58] have reviewed Canadian spent fuel storage tests in which this process occurred (at 150°C), and Taylor and coworkers have studied the oxidation of unirradiated UO_2 in air–steam mixtures (generally above 200°C) [59–61]. A critical finding of these studies was that oxidation occurred preferentially in the grain boundaries, a process that could eventually lead to breakup of the fuel pellets. This preferential grain boundary attack seemed particularly evident in spent fuel specimens in which it may have been exacerbated by radiolytic effects [62].

In the fuel storage experiments at 150°C, the oxidation product was not U_3O_8, as observed after oxidation in dry air at higher temperatures, but a thin layer of U_3O_7 followed by fuel alteration to U(VI) oxide hydrates. In both the short-term tests with unirradiatd UO_2 and the long-term tests with spent fuel these alteration products accumulated within the reactive grain boundaries. In the spent fuel tests some evidence existed to suggest their formation in the confined volumes within grain boundaries stiffled the fuel oxidation/dissolution process.

Under fully immersed conditions, the effect of preoxidation on the fuel dissolution rate appears to be minor [55]. Prior to immersion, spent fuel specimens (ATM-105, a moderate burnup, low fission gas release fuel, and ATM-106, a high burnup, high fission gas release fuel) were pre-oxidized in air at 110–200°C to give surface stoichiometries of $\sim UO_{2.4}$(U_4O_{9+x} with no indication of U_3O_8 formation). The influence of this treatment on the corrosion rate of ATM-105 was minor and that of ATM-106 increased by a factor of $\sim$5. It was proposed that this increase was due to the greater accessibility for preoxidation of the grain boundaries in this high fission gas release fuel. For unirradiated UO_2 the increase in dissolution rate on oxidation to U_3O_7 and U_3O_8 was only a factor of 2–4 once the increase in

surface area on oxidation to U_3O_8 was accounted for. More recently, Gray [63] showed that there was little difference in the dissolution rates of three different preoxidized (up to U_4O_{9+x}) spent fuel specimens.

Steward and Mones [54] reported corrosion rates for UO_2, U_3O_8 and dehydrated schoepite, UO_3H_2O, measured using the single-pass, flow-through system. The order of rates was

$$R_{UO_3\cdot H_2O} \gg R_{U_3O_8} > R_{UO_2}. \quad (10)$$

For $UO_3 \cdot H_2O$ the rate was at least an order of magnitude higher than for U_3O_8, while that for UO_2 was only a factor of 2 less than for U_3O_8. The rate for $UO_3 \cdot H_2O$ was also strongly dependent on $[CO_3]$, consistent with the strong dependence on carbonate of the dissolution of soddyite, another fully oxidized uranium oxide ($(UO_2)_2SiO_4 2H_2O$)) [64].

This marginal effect of preoxidation up to the U_3O_8 stage is not surprising in view of the mechanism for UO_2 dissolution presented above for oxidizing conditions. The preoxidation of UO_2 to $UO_{2.33}/UO_{2.4}$ (Section 3.1) guarantees that, irrespective of the surface stoichiometry prior to exposure to water, the fuel surface achieves effectively the same composition that would be established by the aqueous oxidation of non-preoxidized fuel before dissolution commences. Since corrosion potential measurements indicate that this preoxidation step ($UO_2 \rightarrow UO_{2.33}$) also occurs on spent fuel [39] prior to dissolution, it is unlikely that unirradiated UO_2 and spent fuel will exhibit significantly different corrosion rates. This issue will be addressed in more detail below.

It can be concluded that preoxidation will not lead to an increase in the intrinsic dissolution rate of spent fuel under oxidizing conditions, although the overall U release rate could increase if preoxidation in moist air leads to preferential oxidation of the grain boundaries and, hence, to the exposure to groundwater of a greater surface area of fuel.

5.3. Effect of pH

Based on the discussion in Section 3.1.1 above, no significant influence of pH on corrosion rate would be anticipated in the range $5 \leqslant pH \leqslant 10$ likely to prevail in all repositories except those inundated with saturated Mg-containing brines (when a $pH < 5$ is expected). Within this pH range, the solubility of the U(VI) corrosion product is at a minimum and independent of pH [65]. This independence of corrosion rate on pH is clearly shown in the measurements of Thomas and Till [66] using UO_2 fuel pellets, as well as in the more extensive series of experiments in which dissolution rates measured on U_3O_8 were compared to previously measured rates on UO_2 and spent fuel [54]. Based on regression fits to their data set obtained in a statistical set of experiments over the pH range 8–10, Steward and Mones [54] obtained the following relationships for dissolution rates (r in mg m^{-2} d^{-1}).

$$\begin{aligned}
\log r_{U_3O_8} &= 7.951 + 0.6492\log[CO_3] \\
&\quad + 0.1065\log[H^+] - 1333\ T^{-1} \\
\log r_{UO_2} &= 5.825 + 0.2260\log[CO_3] \\
&\quad - 0.1571\log[H^+] - 1734\ T^{-1} \\
\log r_{SF} &= 7.202 + 0.2260\log[CO_3] \\
&\quad + 0.0905\log[H^+] - 1628\ T^{-1}
\end{aligned} \quad (11)$$

From these expressions it is clear that, for all forms of uranium oxide investigated, the dependence on pH is minor to insignificant.

5.4. Dependence on O_2 concentration

Fig. 29 shows the dependence of corrosion rate on dissolved oxygen concentration determined by different researchers for a range of solution conditions. In neutral carbonate solutions, Tait and Luht [14] and Steward and Weed [67] obtained a reaction order of ~0.7 and a similar value was obtained for pH = 4.5 in $MgCl_2$ brine [32], although in the last case the actual corrosion rates are significantly lower. Based on electrochemical measurements of current–potential relationships in carbonate solutions, a reaction order between 0.67 and 0.8 is predicted [27], in excellent agreement with measurements. At odds with these values is the reaction order measured electrochemically (based on the procedure in

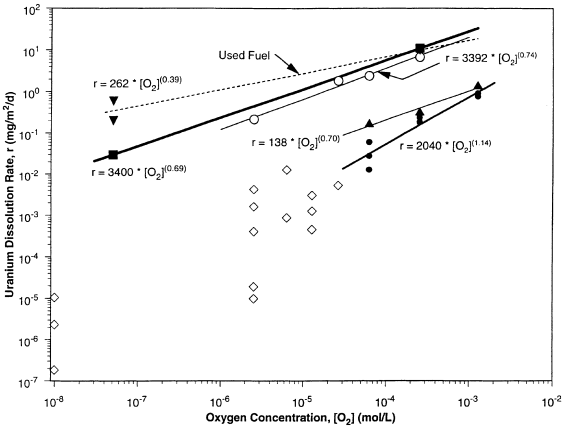

Fig. 29. UO_2 and spent fuel dissolution (corrosion) rates as a function of oxygen concentration measured by different methods in different environments: (●◇) from electrochemical measurements in 0.1 mol l^{-1} $NaClO_4$ (pH = 9.5) using the procedure outlined in Fig. 18 [16]; UO_2(■) and spent fuel (▼) rates measured in 0.01 mol l^{-1} NaCl (pH ~ 9) [14]; (▲) UO_2 rates measured in $MgCl_2$ brine (pH = 4.5) [32]; (○) UO_2 rates measured in 0.02 mol l^{-1} $NaHCO_3$ (pH ~ 9) [67]. The equations represent the best fits to the data.

Fig. 18) in non-complexing neutral solutions, Fig. 29, when a reaction order of ~1 was obtained. Thomas and Till [66] in neutral granitic groundwater, Grambow et al. [68] at pH = 7.7 in NaCl, and Grandstaff [69] in neutral water, also measured a first-order dependence on O_2 concentration.

There appears to be a clear distinction in these measurements between the reaction order determined in complexing and acidic solutions, when dissolution of UO_2^{2+} occurs directly from a 'clean' UO_2 surface, and that recorded in non-complexing neutral solutions, when dissolution occurs from a $UO_{2.33}$ surface and there is a strong possibility that the corrosion product deposits could, at least partially, block the fuel surface. Exposure of the UO_2 surface allows O_2 reduction to be catalyzed by the U(VI) and/or U(V) sites present on the fuel surface (Fig. 19(A)). If these sites are partially blocked, then it is possible that this could lead to the polarization (retardation) of the O_2 reduction reaction, which would be manifested by a decrease in the log current–potential slope and, hence, an increase in the reaction order. Such a retardation of the O_2 reduction reaction has been observed electrochemically when small amounts of corrosion product deposit are present on the fuel surface [41].

The reaction order with respect to O_2 for spent fuel is lower than for UO_2, Fig. 29. This is due to the increased rate measured at the lowest O_2 concentration. Tait and Luht [14] attribute this to the support of corrosion by radiolysis which is more apparent at the lower O_2 concentration. An even more marked suppression of any dependence on $[O_2]$ was observed for the corrosion of LWR fuel by Steward and Gray [70]. At room temperature, the rate was almost independent of O_2. While a suppressed reaction order with respect to O_2 is consistent with a radiolytic effect, the total absence of any dependence suggests other unknown factors may also be involved.

5.5. Dependence on carbonate concentration

Fig. 30 shows a comparison of corrosion rates as a function of carbonate concentration measured using the single-pass flow-through apparatus and electrochemically using the procedure outlined in Fig. 18. Except for the early preliminary electrochemical data [15], the reaction order with respect to carbonate is 0.4–0.6. The order predicted electrochemically by the same procedure used to predict the reaction order with respect to O_2 is 0.33–0.4 [27]. Both measured and predicted values are consistent with the previously published literature values of 0.53 [71] and 0.46 [72]. In single-pass flow-through experiments at very low O_2 concentration (2 ppb), Tait and Luht [14] clearly showed that there was no dependence of the corrosion rate on carbonate concentration.

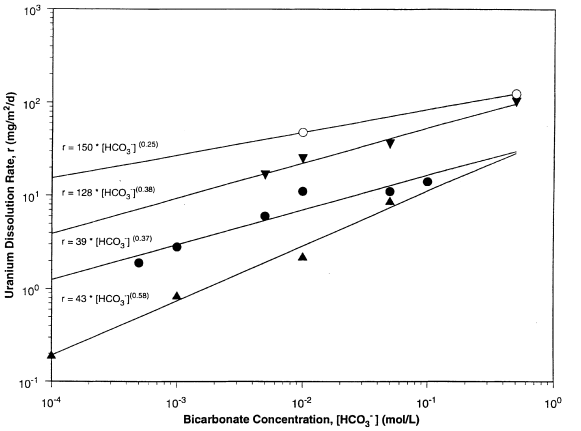

Fig. 30. UO_2 dissolution (corrosion) rates as a function of HCO_3^- concentration in aerated solutions at 25°C: (●) measured in aerated HCO_3^- solution containing 0.1 mol l^{-1} NaCl (pH ~ 9) [14]; (▲) [52]; (○) preliminary UO_2 rates determined electrochemically in 0.1 mol l^{-1} $NaClO_4$ (pH = 9.5) [15]: (▼) from electrochemical measurements in 0.1 mol l^{-1} $NaClO_4$ (pH = 9.5) using the procedure outlined in Fig. 18.

While this agreement between experiment and prediction is gratifying, it hides a host of issues when trying to define a single reaction order to express the dependence of corrosion rate on carbonate concentration. Since carbonate is a strong complexing agent for UO_2^{2+} but not for U^{4+}, which is preferentially hydrolyzed (Table 6.1 in [4]), it would not be expected to accelerate corrosion significantly under marginally oxidizing conditions as observed. However, this means that the dependence on carbonate will change with redox conditions; i.e. the rate of oxidation to produce UO_2^{2+} will become more rate determining as conditions become less oxidizing and the dependence of the overall corrosion rate on $[CO_3]$ will decrease.

A second well-documented change in the dependence of the rate on carbonate concentration occurs with temperature. An increase in temperature to only 40°C changes the reaction order from the room temperature (20–25°C) value of 0.4 to a value of 0.6–0.7 [52,66]. This has been shown by de Pablo et al. [18] to be due to a switch in the rate determining step from the rate of surface oxidation to the rate of U(VI) ion transfer to solution, the latter being a step aided by complexation with carbonate. In corrosion science terms it would be said that control of the overall corrosion process had switched from the cathodic (O_2 reduction) to the anodic (UO_2^{2+} dissolution) reaction.

These complications are undoubtedly reflected in the relatively low dependence of the corrosion rate on carbonate obtained by Steward and Mones [54], Eq. (11), based on a fit to a data set which encompasses many of these mechanistic changes within the range of the

experimental design of parameters (i.e., $25°C \leqslant T \leqslant 75°C$; 2×10^{-4} mol $l^{-1} < [HCO_3] < 2 \times 10^{-2}$ mol l^{-1}).

As expected, Steward and Mones [54] found that the dependence on $[CO_3]$ of the corrosion rate increased in the order

$$r_{SF} < r_{UO_2} < r_{U_3O_8} \ll r_{UO_3 \cdot H_2O}. \quad (12)$$

This combination of a lower dependence of spent fuel corrosion rate on both $[CO_3]$ and $[O_2]$ (see previous section) compared to those obtained on unirradiated UO_2 suggests the rate of oxidation of spent fuel may be lower than that of UO_2. However, the similarities in corrosion rates for these two specimens indicate different balances in the kinetics of the anodic and cathodic reactions do not have a major effect overall. The difference in reaction orders with respect to carbonate between UO_2 and U_3O_8 clearly indicates that the anodic reaction (UO_2^{2+} dissolution) is slower than the cathodic reaction (O_2 reduction) at room temperature. This is not surprising considering oxidation of only one in three U atoms is required for corrosion in the case of U_3O_8. Additionally, for this solid two oxidized uranium species already exist within the solid as UO_2^{2+} entities [4] and their transfer to solution in a reaction involving carbonate would be expected to be rapid, a process that could subsequently facilitate oxidation of the remaining U(IV) atom. This would suggest that the observed increase in corrosion rate of U_3O_8 compared to UO_2 (a factor of 3–5) is a real difference in intrinsic dissolution rate.

The extremely high (relatively speaking) dissolution rate of $UO_3 \cdot H_2O$ and the strong dependence on carbonate concentration reflect both the thermodynamic driving force provided by the increased solubility due to complexation of UO_2^{2+} by carbonate, reactions (7b) and (7d), and the absence of any need for an oxidation step; i.e. this is chemical dissolution not a corrosion reaction. A similar strong dependence of dissolution rate on carbonate concentration was observed for the U(VI) containing phase, soddyite [64]. This particularly strong dependence of dissolution rate for fully oxidized U phases on carbonate illustrates that the primary influence of carbonate will be to prevent the deposition of corrosion product deposits. The influence of carbonate on the intrinsic corrosion rate of the fuel is less marked but still a significant influence over the concentration range $10^{-4} \geqslant [CO_3] \geqslant 10^{-1}$ mol L^{-1}.

5.6. Influence of temperature

An early review of the literature [16] showed that the activation energy ($E_A^{\ddagger}$) for UO_2 corrosion depended very much on the environment in which the measurements were made. When measured in acidic solutions, generally with oxidants such as Fe(III), V(V) and H_2O_2, values in the range 50–67 kJ mol^{-1} were obtained. For carbonate solutions in the pH range 8–10, and usually with the oxidant O_2, the range of values covered 42–63 kJ mol^{-1}. In non-complexing neutral solutions, the range of measured values was significantly lower, 29–34 kJ mol^{-1}. Recent measurements have proven consistent with these classifications. An activation energy of 47 kJ mol^{-1} was measured in aerated carbonate solutions using the single-pass flow-through technique [14]. Thomas and Till [66] and Park and Lee [73] obtained values of 20 kJ mol^{-1} and 26–31 kJ mol^{-1} in distilled water and in a borate-buffered granitic groundwater (pH = 6), respectively. In granitic groundwater (containing 2130 mg l^{-1} of Ca^{2+}) Thomas and Till [66] actually found a suppression of the corrosion rate with temperature, an observation attributable to the formation of a mineralized deposit. The formation of such adherent mineral deposits leading to the blockage of fuel dissolution at 90°C in a Mg^{2+}-containing groundwater was also observed by Lahalle et al. [74].

The evidence for the formation of secondary deposits at higher temperatures suggests that the low activation energy obtained in non-complexing neutral groundwaters can be attributed to the partial suppression of dissolution by the accumulation of a corrosion product deposit. The acceleration of dissolution by an increase in temperature would be counterbalanced by the increased accumulation of U(VI) phase deposits, especially if the latter have an inverse dependence of solubility on temperature [75]. An attempt to depict this effect schematically is shown in Fig. 31(A). By contrast, in carbonate-containing solutions, corrosion product deposition is prevented and activation energies more typical of an uninhibited oxide dissolution process are obtained (40–100 kJ mol^{-1}; [5,76], Fig. 31(B).

This explanation, however, ignores the changes shown to occur in the underlying layer as the temperature increases. Using Rutherford backscattering, Matzke and Turos [21] and Matzke [22] showed that the thickness of $UO_{2.33}$ layer increased from 5 to 8 nm at room temperature to a few hundred nm (100–500 nm, depending on temperature and time of exposure) for temperatures between 150°C and 200°C. These film thicknesses were not measured under steady-state conditions and it is likely that even thicker films would eventually form. A dependence of thickness on the square root of time (t) was observed at these temperatures, consistent with control of the oxide growth by O^{2-} diffusion through the surface $UO_{2.33}$ layer. Unfortunately, no estimate of film thicknesses has been made for the intervening temperature range of most interest to fuel dissolution processes.

In carbonate solutions, the influence of temperature is more complex than illustrated in the simple schematic in Fig. 31(B). Steward and Mones [54] noted when

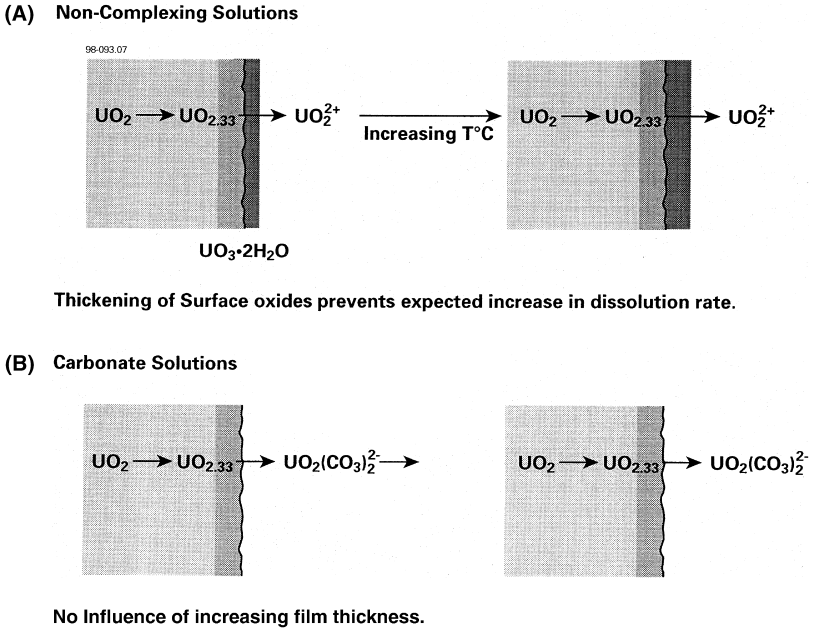

Fig. 31. Schematic diagrams illustrating the different effects of temperature on UO_2 dissolution (corrosion) in (A) non-complexing and (B) carbonate-containing solutions.

fitting a large data set obtained from a statistical design of experiments that temperature and carbonate concentration showed a significant interaction and that the addition of cross terms for these interactions substantially improved their data fit. They also noted that the influence of carbonate increased with temperature. This is not surprising since de Pablo et al. [18,52] have shown that a number of mechanistic features of the dissolution process change with temperature and carbonate concentration. For a sufficiently high carbonate concentration, the intermediate $UO_{2.33}$ layer does not form, a feature not incorporated in the simple schematic in Fig. 31(B). They have also shown that a change in mechanism occurs over the temperature range 20–75°C, making any activation energy determined over this range only an apparent value.

5.7. Effect of water radiolysis

5.7.1. β/γ-Radiolysis

Fig. 32 compares corrosion rates for unirradiated UO_2 measured as a function of γ-dose rates in aerated/oxygenated solutions. This plot includes data from electrochemical experiments [16], single-pass flow-through experiments [14] and data from the literature [45,77]. Although included in the figure the data of Gromov in alkaline carbonate solutions seem unrealistically low and are not considered further. The dependence of corrosion rate on dose rate is expressed empirically, by the slope of these plots. While the dependence observed by Gromov is similar to that determined electrochemically, that from single-pass flow-through measurements is higher.

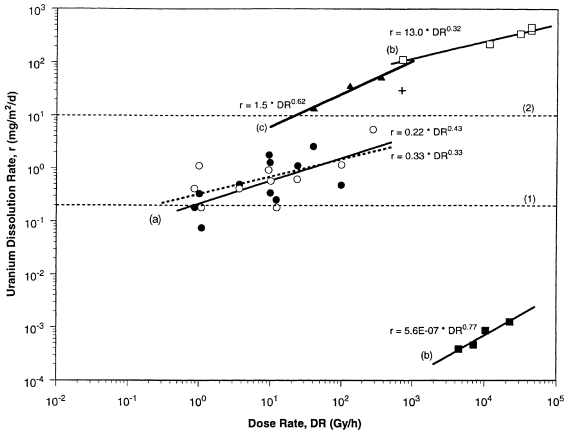

Fig. 32. Dissolution (corrosion) rates (r) of unirradiated UO_2 in irradiated, aerated/oxygenated solutions as a function of gamma dose rate (DR): (a) rates obtained electrochemically in aerated 0.1 mol l^{-1} $NaClO_4$ (pH = 9.5) solutions [16]; (b) rates measured in acidic sulphate solutions (pH ~ 1) and alkaline carbonate solution (pH ~ 10) [77]; (c) rates measured in 0.1 mol l^{-1} NaCl + 0.01 mol l^{-1} $NaHCO_3$ (pH ~ 8.5) [78]; (+) measured in oxygenated solution (pH ~ 8.2) [45]. The horizontal dashed lines show the rate predicted for unirradiated aerated solution (1) and the rate measured in flow-through experiments in aerated bicarbonate solution (2). The equations represent the best fits to the data.

Unfortunately, rates from the different sources cannot be straightforwardly compared since they are all recorded under different chemical conditions. The rates measured by Tait and Luht [14] in carbonate solutions are $\sim 10^2$ times higher than those predicted from electrochemical measurements in non-complexing solutions. This is approximately the difference between the rates in these solutions in the absence of radiolysis, Fig. 29. The horizontal lines labelled 1 and 2 in Fig. 32 show the electrochemically determined rate for unirradiated aerated solution containing no carbonate (from Fig. 29), and the rate measured in flow-through experiments in unirradiated aerated carbonate solutions (from Fig. 30). The intersection of these lines with the fitted lines for the rates in irradiated solutions indicates that the influence of gamma radiation on the corrosion rate becomes negligible for dose rates $\leqslant 1$ Gy h^{-1} in aerated non-complexing solutions, and $\leqslant 10$ Gy h^{-1} in aerated carbonate solutions.

A number of authors have noted that experiments designed to determine whether any difference in intrinsic dissolution rate exists between UO_2 and spent fuel are inevitably compromised by the radiolysis effect. As discussed above, Tait and Luht [14] attributed the low dependence of the spent fuel corrosion rate on $[O_2]$ to the distortion of the data at the lowest $[O_2]$ by the radiolytic production of oxidants. Loida et al. [9,78] showed unequivocally that radiolysis in experiments with spent fuel specimens was sufficient to maintain oxidizing conditions no matter what precautions were used to achieve anoxic conditions. In these last experiments, various spent fuel surface area to solution volume ratios were used. From the variations in corrosion rates with the surface area to volume ratio they showed that, as the available surface area increased, the efficiency of consumption of radiolytic oxidants increased leading to a limitation in the corrosion rate as radiolytic oxidants became locally depleted in concentration.

This clear radiolysis effect makes it injudicious, at best, to use the results obtained in experiments with spent fuel to interpret the long term behaviour of this fuel when such radiolytic effects will be absent. In this regard, it is important to know whether the radiation effect observed in short-term tests is due to β/γ or α-radiolysis, since the former decay to insignificant levels in <1000 years while the latter can persist for many thousands of years, Fig. 6. Unfortunately, for experiments with spent fuel it is difficult to decide. Based on their measured rates as a function of fuel surface area to solution volume ratio, Loida et al. [9,78] claimed that α-radiolysis was most important. However, their claim that corrosion was predominantly due to radiolysis was based on a comparison of fuel alteration rates to the rate of radiolytic gas production, a process taken to be caused predominantly by γ-radiolysis.

Fig. 33 shows a series of E_{CORR}–time plots recorded on various spent fuel specimens exposed to aerated neutral solutions. The characteristics of the fuels are given in Table 1. Also shown in the figure is the response of a UO_2 electrode placed inside and outside the hot cell. The most positive $(E_{CORR})_{SS}$ correlates with the fuel with the highest $\beta + \gamma$ dose rate. Since this fuel has the lowest α-dose rate, the clear implication is that the β/γ fields are responsible for the very rapid oxidation of this electrode (i.e., the fast rise of E_{CORR} to steady-state) and the establishment of the final very positive $(E_{CORR})_{SS}$ value. This claim is strongly supported by the observations made with the unirradiated UO_2, when the effects

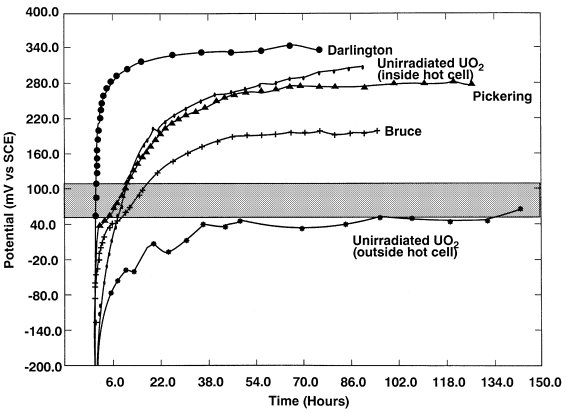

Fig. 33. Corrosion potential (E_{CORR}) of three used fuel electrodes as a function of time of immersion in an aerated solution of 0.1 mol l^{-1} $NaClO_4$ (pH $\sim$ 9). The characteristics of these three fuels are given in Table 1. Also shown is the E_{CORR} for an unirradiated UO_2 electrode measured inside and outside the hot cell. The shaded area shows the range of $(E_{CORR})_{SS}$ generally observed for unirradiated UO_2 in the absence of any radiation field.

Table 1
Characteristics of used fuel specimens used to construct electrodes

Fuel			Dose rates (Gy h^{-1})		
Reactor bundle	Burn up (GJ (kg U)$^{-1}$)	Cooling time years	α	β	γ
Darlington L23139C	425	1.0	33.1	7734	260.6
Pickering PA07993W	880	15.0	15.0	125.3	401.3
Bruce BF21271C	970	13.1	160.9	507.1	31.4

of α-radiation are definitely absent. When placed in the hot cell and exposed to predominantly γ-radiation a much more positive $(E_{CORR})_{SS}$ value is achieved than in the absence of radiation. E_{CORR} values >300 mV are sufficient to place the fuel in the potential region where the establishment of local acidic conditions, leading to grain boundary etching and pitting, is possible, Fig. 10. The fact that such positive potentials can be achieved with an external gamma source when no α-field is present, but cannot be achieved in the presence of a substantial α-dose rate is solid evidence to support a contention that it is the β/γ, not the α-radiolysis, which is most aggressive.

A second set of experiments with spent fuel electrodes showed that these positive excursions in E_{CORR} can be almost instantaneously reversed by the addition of carbonate, Fig. 34. A similar effect could be produced on an unirradiated UO_2 electrode exposed to an external gamma source [39]. At the time the rapid drop in E_{CORR} on addition of carbonate was attributed to the rapid re-dissolution of a thin and/or localized deposit of U(VI) phases. While such a re-dissolution process undoubtedly did occur, the rapidity with which E_{CORR} changes could be more plausibly attributed to the neutralization of local acidity. Once carbonate had been added and the pH excursion prevented, the response of E_{CORR} to the removal of the field was minor. This confirms that the maintenance of local chemical conditions (i.e. a low pH stabilized within a porous U(VI) deposit, Section 4.3) is critical to the achievement of a high E_{CORR} value.

This accumulation of evidence suggests that the very aggressive attack of spent fuel specimens in unsaturated drip tests is also attributable to the influence of β/γ fields although the authors have claimed it is due to α-radiolysis [79–81]. In the early stages of these tests (up to 60 days, [79]), the original pH = 8 was found to be suppressed to as low as 4 in some leachate samples. While it can be argued that this is due to the radiolysis of moist air leading to the fixation of H in acidic species (e.g. HNO_3) in these tests with limited amounts of water, the experiments under fully immersed conditions, described above, show this process is not a prerequisite for the establishment of acidic conditions.

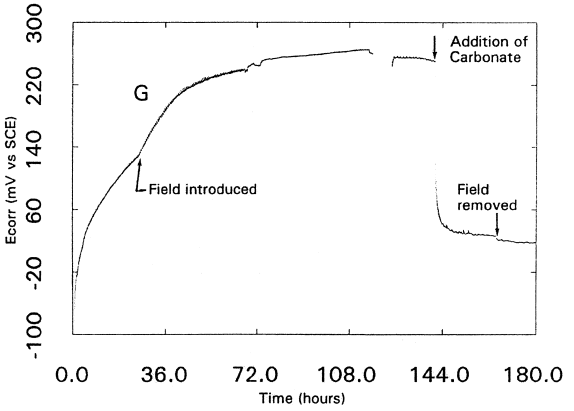

Fig. 34. Corrosion potential (E_{CORR}) recorded on a used fuel electrode (burnup 780 GJ/kgU; cooling time 16.8 years) as a function of time in 0.1 mol l^{-1} $NaClO_4$ (pH = 9.5) showing the response to the introduction and removal of an additional γ-radiation source (~5.6 Gy/h ≡ 560 R/h) and the addition of sodium carbonate to a concentration of 0.1 mol l^{-1} [39].

After 3.7 years the surface was covered with a clear layer of corrosion deposit, an inner layer of a uranyl silicate phase which was dense and tightly adherent to the fuel surface, and an outer, less dense layer which was easily dislodged. The inner layer was 5–10 μm and the outer layer 10–30 μm in thickness. Both layers were sodium boltwoodite ($Na[(UO_2)(SiO_3OH)] \cdot H_2O$), although Cs and Mo, released from the fuel, were trapped in a Cs–Mo–uranyl solid ($((Cs_{0.9}Ba_{0.55})[(UO_2)_2(MoO_2)O_4(OH)_6] \cdot 6H_2O$). The inner layer showed several curvilinear features, some of which appeared to be pre-existing grain boundaries suggesting a pseudomorphic replacement of the spent fuel by sodium boltwoodite. The continuing release of Tc over the duration of the experiment indicated that the presence of these alteration layers did not protect the underlying fuel from further corrosion. Examination of cross-sections showed that dissolution had penetrated deep into grain boundaries. The absence of secondary deposits in the grain boundaries showed uranium from these sites had been transported out of the grain boundaries, through the inner layer, and either deposited in the outer layer or transported away from the surface in the leachate. Given the pseudomorphic relationhip between the fuel and the inner layer it seems doubtful that significant precipitation of dissolved U from the grain boundaries occurred within this layer.

All this evidence suggests the development of acidity at the fuel surface and within the grain boundaries. Acidity would seem an essential requirement for the maintenance of open grain boundaries in the fuel and pores within the inner layer, and the prevention of uranyl phase precipitation until the outer regions of the outer layer were reached. The E_{CORR} at the fuel surface, and within the grain boundaries was estimated by considering the E_h required to form soluble ions of the elemental components of the ε-phase (Tc, Mo, Ru, Rh, Pd) based on E_h–pH diagrams. Since Ru dissolution was observed, E_{CORR} must have been as high as 0.6 V (vs SHE) or 0.36 V(vs SCE). This is sufficiently positive for acidic conditions to be established at the fuel surface, Fig. 10. Fig. 10 also indicates that such positive values of E_{CORR} have only been achieved in the presence of high β/γ fields. While this does not rule out the possibility of establishing such aggressive conditions by α- radiolysis, especially within the confined spaces within grain boundaries, it would appear an unlikely scenario, given

the redox buffering effect which occurs with this form of radiation, Section 4.4. A possibility which cannot be ruled out, but has not been considered, is that a combination of α- and β-radiolysis (both short range radiation effects) could combine to convert the H_2O_2 produced by α-radiolysis into a high local concentration of radical oxidants. Even if this proved to be a functional mechanism it would remain important only as long as β-fields were maintained.

It can be concluded, though not considered proven, that the aggressive fuel corrosion observed in the unsaturated drip tests will not be observed once β/γ fields have decayed, and that the unsaturated drip tests do not represent the behaviour to be expected on spent fuel in the long term (i.e. beyond a few hundred years).

5.7.2. α-radiolysis

Measurements of E_{CORR} as a function of α-source strength, described above in Section 4.4, show that the influence of α-radiolysis on fuel oxidation and dissolution is dominated by the production of the molecular oxidant H_2O_2, and its decomposition to O_2 and H_2O_2. This leads to a redox buffering effect which renders the corrosion rate independent of α-source strength (and hence α-dose rate) for strengths (S_α) $\geqslant$ 250 μCi, Fig. 35 [38].

The data plotted in Fig. 35 have been used in the assessment of spent fuel performance under Canadian repository conditions [11]. These calculations claimed that the influence of α-radiolysis on fuel corrosion would be totally negligible. However, this prediction relied on the extrapolation of the rates plotted in Fig. 35. Despite the elimination of some of the less realiable data points recorded at low source strengths, this extrapolation remains, at best, very approximate, since no reliable and mechanistically justified function exists to fit the data in this figure. In fact, based on the understanding of the α-radiolysis effect (Section 4.4) the data in Fig. 35 should be divided into two distinct regions. For $S_\alpha \geqslant 250$ μCi ($\log S_\alpha = 2.6$ in the figure), the rate is independent of S_α, while for S_α less than this the rate falls drastically as S_α decreases. Our recent calculations [51] give us confidence that the high source strength data are reliable, but since the redox buffering effect makes the rate independent of S_α, these cannot be used as the basis of an extrapolation to predict fuel corrosion rates at the lower source strengths expected in spent fuel.

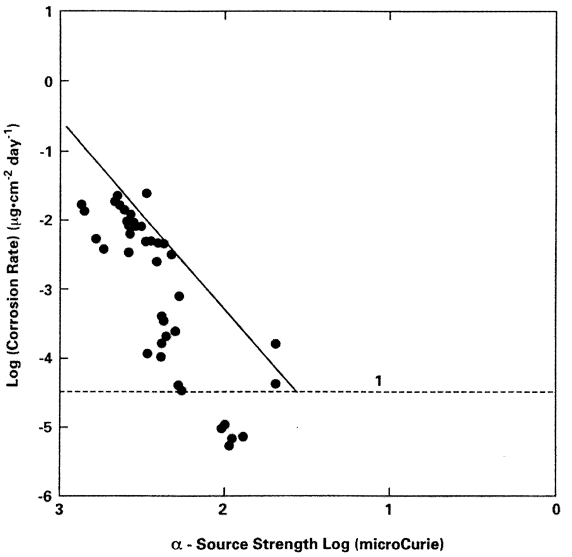

Fig. 35. Corrosion rates of UO_2 as a function of alpha dose rate in solutions undergoing alpha radiolysis in 0.1 mol l^{-1} $NaClO_4$ (pH = 9.5). The solid line is arbitrarily drawn to encompass all the data points except the two suspiciously high ones at low dose rates. The horizontal line at a rate of 3×10^{-5} μg cm^{-2} d^{-1} corresponds to a limit below which the data cannot be considered reliable [11,38].

Two further points are worth emphasizing for α-radiolysis effects. At high source strengths, the redox buffering effect appears to restrain E_{CORR} to the value achievable in aerated solutions. Consequently, for an aerated environment, such as the one expected in Yucca Mountain, the influence of α-radiolysis will not exceed that achieved by dissolved oxygen alone. Secondly, the possibility that α-radiolysis could produce locally acidic conditions requires that the H_2O_2 produced radiolytically be retained on the fuel surface and not lost by transport to the environment. For the limited wetness expected within Yucca Mountain there is a higher probability of this process occurring than under fully immersed conditions. The measurements described in [38,50] clearly indicate this is an unlikely prospect, only possible at high source strengths and confined geometries. As the α-fields decay, the tightness of the reaction site required to sustain this effect would increase; i.e. narrower apertures would be required.

5.8. Comparison of spent fuel and unirradiated UO_2

With the exception of the radiolysis effect, differences in surface area and, possibly, the greater accessibility of grain boundaries, there is little evidence to suggest that the corrosion of spent fuel is intrinsically a different process to that on unirradiated UO_2. If such an effect does exist then it is marginal and accounted for by an increase in rate by only a factor of 2 or so. This does not mean to say there are no differences in properties between the two fuel forms, only that, when considered together, they make little difference.

Electrochemical evidence [29,39,82] shows that the basic mechanism of fuel dissolution is the same for UO_2 and spent fuel. The establishment of a thin oxidized surface layer ($UO_{2.33}/UO_{2.4}$) appears to enforce a similar reactivity on both materials by disguising the

different chemical features of the underlying surfaces from the corrosion environment. Those compositional features, which are different between the two forms, appear to make little difference, perhaps for this reason. Thus, Bottomley et al. [29] confirmed that in-reactor changes (such as rare earth doping) reduced the resistivity of the fuel by a factor of 10–20, but this made only a factor of 2 difference in corrosion rate. Using SIMFUELS, Betteridge et al. [23] showed that the introduction of the ε-phase did not accelerate corrosion by catalyzing the slow O_2 reduction reaction since this noble metal alloy was passivated under oxidizing conditions. Loida et al. [78] showed that the corrosion rate of the fuel rim, where higher fission gas mobilities and higher radionuclide inventories exist, did not differ significantly from that of the bulk of the fuel.

Steward and Gray [70] systematically compared the corrosion rates of UO_2 and spent fuel (ATM 103, 33 MWd/kg U) over a range of O_2 and carbonate concentrations, pH and temperature. On average the UO_2 corrosion rate was approximately a factor of 3 greater than that of the spent fuel. Since this was about the difference in UO_2 corrosion rates in inter-laboratory tests, (Section 5.1) they concluded that the differences between UO_2 and spent fuel were probably insignificant. Subsequent studies [63] covering the burnup range 30–50 MWd/kg U reached the same conclusion. Most of the results from these tests were fitted to produce the relationship given above in Section 3.1.2. In general the dependence of the spent fuel corrosion rate was less dependent on O_2 and carbonate concentrations and similarly influenced by temperature. While it is possible that any real dependence on O_2 concentration is obscured by the influence of radiation fields in the spent fuel measurements [14], these measurements confirm that there is no major difference between UO_2 and spent fuel corrosion rates. If anything, for reasons not totally understood, the rate appears to be slightly lower for spent fuel.

A significant potential difference between UO_2 and spent fuel is the potential for pellet break-up, especially if subjected to a period of moist air oxidation prior to exposure to groundwater (Section 5.2). Based on comparisons of surface area measurements by different techniques it was concluded that while the grain boundaries in UO_2 were tight enough to preclude significant penetration by water, those of spent fuels were not [83]. Various estimates have been made on the importance of grain boundary dissolution and leaching from spent fuels. Gray et al. [12,55] and Stroes-Gascoyne et al. [84] have shown that penetration of grain boundaries by solution is not universal, and is confined to only a few grains in depth.

For CANDU fuel exposed to oxidizing solutions for 19 years [84] grain boundary dissolution was observed only at the base of narrow cracks and was confined to the outer rim area where residual porosity and sintering defects are to be expected. Attack appeared to have occurred to a depth of ~5–10 grains, consistent with the claim by Gray et al. [12,55] that grain boundaries in LWR fuels could be accessible for dissolution to a depth of between 2 and 9 grains from the surface. The importance of the grain boundary is clearly indicated in the case of 19-year leached CANDU fuel, for which no grain boundary attack was observed in the mid-pellet region of the fuel, even where extensive fuel fracturing and micro-cracking existed as a result of high fuel operating temperatures in this region.

As discussed above in Section 5.2, pre-oxidation could have a significant effect on fuel corrosion rates, not by changing the intrinsic corrosion rate, but by allowing solution to penetrate grain boundaries. Gray [63] clearly showed this to be the case. Oxidation (to U_4O_{9+x} at 175°C in air) did not affect the intrinsic corrosion rate of three different fuels, but in one case, penetration of the grain boundaries was very extensive. No dependence of corrosion rate on burn up was detected, although the range investigated was narrow.

5.9. Formation of corrosion product deposits and the retention of radionuclides

The hope is that the formation of corrosion product deposits will affect the fuel dissolution process in two ways:

1. it will block the fuel corrosion process;
2. deposits will retain radionuclides released by fuel corrosion, thereby preventing, or at least delaying, their release to the repository.

Blockage of the fuel corrosion process could take a number of forms. The development of a low porosity deposit would impede the transport of oxygen to the fuel surface possibly leading to less oxidizing conditions than expected. It would also decrease the surface area available for corrosion by an extent related to the porosity of the deposit. Whether or not radionuclides are retained by the corrosion product deposit will depend on the structural compatibility of the host matrix (inevitably a U^{VI} phase) for a particular radionuclide, the kinetics and mechanism of co-precipitation processes, the ratio of the surface area to available solution volume, and the local convective and diffusive conditions.

A substantial body of evidence exists to show that corrosion product deposits form under both moist vapour and fully immersed conditions. In the section on pre-oxidation, the accumulation of deposits was shown to occur in the grain boundaries under moist vapour conditions and evidence existed to suggest they may block the corrosion/alteration process. Buck et al. [85] characterized the nature of the deposits formed in aerated vapour at 90°C on spent fuel as dehydrated schoepite ($UO_3 \cdot 0.8H_2O$) with a small amount of a

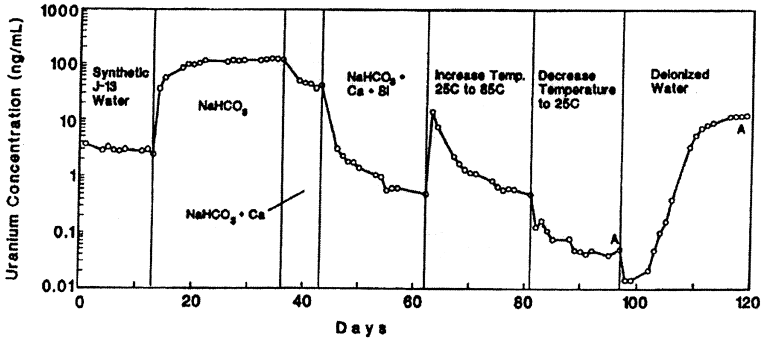

Fig. 36. Uranium concentrations measured in a flow-through experiment with unirradiated UO_2 pellet fragments showing the effect of adding 15 mg l^{-1} of Ca^{2+} to a 2×10^{-3} mol l^{-1} HCO_3^- solution (at 36 days) followed by the further addition of 30 mg l^{-1} SiO_4^{4-} (at 43 days). Measurements performed using the single-pass flow-through technique [87].

Cs–Mo uranyl oxide hydrate [86]. After 924 days of exposure the thickness of the deposit was 100–200 μm. No evidence was presented to suggest that the alteration process was slowing with exposure time under fully immersed conditions. The addition of Ca^{2+} and SiO_4^{4-} exerts a major influence on the fuel corrosion rate. Fig. 36 shows that the addition of 15 mg l^{-1} of Ca^{2+} to a 2×10^{-3} mol l^{-1} HCO_3^- solution decreases the concentration of U in the effluent solution by a factor of 3 in a single-pass flow-through experiment with UO_2. The subsequent addition of 30 mg l^{-1} of SiO_4^{4-} increases this suppression by a further factor of 100. Auger analysis of the UO_2 surface indicated a thin (5–10 μm) layer containing Ca and Si was present on the surface, despite the use of the flow-through system to prevent deposition. A similar suppression of the UO_2 corrosion rate by a factor of 200 was observed by Tait and Luht [14], using a similar experimental system. As little as 10^{-4} mol l^{-1} $CaCl_2$ was sufficient to achieve this suppression in the presence of 10^2 mol l^{-1} HCO_3^-. These last authors also showed that the corrosion rate of spent fuel and the release rate of radionuclides were suppressed by a similar factor in a groundwater containing Ca^{2+} and SiO_4^{4-}, Fig. 37.

The rapidity of the response of the corrosion rate to the addition of Ca/Si, Figs. 36 and 37, indicates that, assuming the ions are incorporated into U(VI) deposits with very low solubilities, very little of these phases is required to suppress corrosion. This is consistent with electrochemical experiments [19] which show that the incorporation of Ca/Si into U(VI) surface phases is very rapid and that only films a few nm thick can suppress dissolution substantially. Corrosion experiments in the presence of γ-radiation fields show that the accumulation of secondary phases, even in the absence of Ca and Si, begins as soon as steady-state corrosion conditions are established, Figs. 16 and 17.

The influence of groundwater species has been investigated in detail in drip tests with UO_2 at 90°C [88].

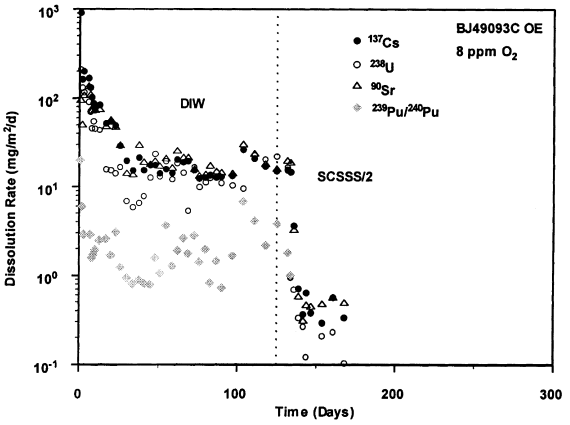

Fig. 37. Dissolution (corrosion) rate of spent CANDU fuel and specific radionuclide release rates at 25°C in distilled deionized water (DIW) and a simulated saline groundwater (SCSSS) containing 0.185 mol l^{-1} Ca^{2+} +0.00027 mol l^{-1} SiO_4^{4-} [14].

These experiments were designed to simulate the conditions anticipated within a failed waste package in the Yucca Mountain repository, and used drip rates of 0.075 m1/3.5 days and 0.0375 m1/7 days of equilibrated J-13 water. The critical components of this water are Ca^{2+} (8.81 mg kg^{-1}), Si (45.4 mg kg^{-1}) and HCO_3^- (135 mg kg^{-1}). Given the relative influences of these species on the corrosion rate, this groundwater could be classed as a Ca/Si dominated water. Since radiolysis effects are absent, and there appear to be few significant differences between the mechanism and rate of UO_2 and spent fuel corrosion, these experiments provide the best picture of the long-term evolution of fuel behaviour under oxidizing conditions. Whether or not they can quantitatively simulate the alteration/corrosion rate of fuel under actual repository conditions depends upon whether the repository conditions (drip rates, temperature, contact water composition) are shown to be close to the test conditions. Intuitively, these experiments appear to

represent very aggressive, and hence conservative, conditions.

Over a transient period of approximately 1–2 years, corrosion was shown to start in the grain boundaries and to eventually lead to the release of fuel grains as a consequence of the convective influence of the drip flow pattern. Attack within the grain boundaries occurred generally to a depth of 2–4 grains, but varied between 0 and 10 grains. This depth of penetration is consistent with the claims of Gray et al. [12,55] that grain boundaries were accessible to a depth of between 2 and 9 grains under fully immersed conditions. Although the evidence is slender, it could be concluded that the large fuel surface area to solution volume prevailing in these drip tests does not lead to any enhancement of grain boundary attack. A more focussed discussion of grain boundary attack in these experiments can be found elsewhere [89].

Beyond this transient period, a dense mat of alteration phases developed on the fuel surface, accompanied by depletion in the alkali and alkaline earth cations and Si in the leachate solution. The nature of these alteration phases and the sequence in which they appear on the fuel are similar to those observed in surficial weathering zones of natural uraninite deposits, with alkali and alkaline earth uranyl silicates being the long-term solubility limiting phases for uranium. The sequence observed is represented schematically in Fig. 38.

The formation of this layer of alteration (or corrosion) products prevents further release of UO_2 particles, hence leading to a drop in the U release rate. However, the approximately constant rate of release over the subsequent 8 years or so of testing shows that the development and transformation of phases does not lead to any observable suppression of the fuel corrosion rate. It is possible that this inability to suppress corrosion is a direct consequence of the convective influence of the drips, since under fully immersed conditions (at 90°C) the transition from a uranyl phase deposit to a protective mineral silicate layer occurs over a period of several weeks [74]. In this latter case the groundwater was a magnesium and silicate containing water, and according

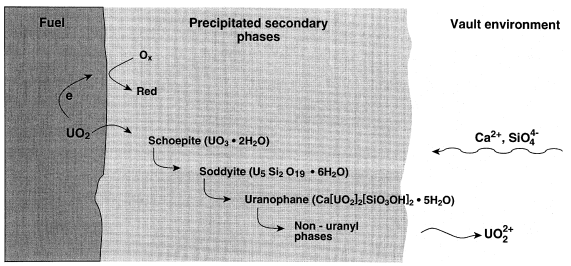

Fig. 38. Reaction sequence showing the alteration of precipitated uranyl phases observed in drip tests with unirradiated UO_2 [88] and expected from observations on surficial weathering zones on natural uraninite deposits.

to the authors, their XPS analyses showed a distinct layering of a U(VI) oxide hydrate under a magnesium silicate layer with no evidence for the incorporation of Mg^{2+}/Si into any U(VI) phase. Experiments in groundwaters containing various amounts of Mg^{2+} and SiO_4^{4-} showed the Si content to be the critical feature determining the formation of this layer. Although the amount of U dissolved over the duration of the experiment was not measured, the U(VI) oxide hydrate layer was very thin suggesting that minimal alteration had occurred. Clearly, a major suppression of fuel corrosion under fully immersed conditions is possible.

Whether or not the formation of alteration phases (corrosion product deposits) will lead to the incorporation and retention of radionuclides released as the fuel corrodes will depend on many factors. Burns et al. [90,91] have shown from crystal structure considerations that the majority of the alteration phases expected to form as the paragenetic sequence is traversed are potential hosts for many radionuclides. For elements such as Np, Pu and Am in the 5+ and 6+ oxidation states, a linear $(An^{5+,6+})O_2^{1+,2+}$(An $\equiv$ actinide) actinyl ion similar to UO_2^{2+} dominates the coordination chemistry, making the incorporation of these elements into uranyl phases probable, although some structural modification would be required to satisfy local bond-valence requirements. The An^{4+} cations should readily substitute for U^{6+} in the sheets that occur in schoepite, ianthinite ($[U_2^{4+}(UO_2)_4O_6(OH)_4(H_2O)_4](H_2O)_5$), becquerelite ($Ca[(UO_2)_3\ O_2(OH)_3]_2(H_2O)_8$), compreignacite ($K_2[(UO)_2)_3O_2(OH)_3](H_2O)_8$), α-uranophane and boltwoodite ($K(H_3O)[(UO_2)(SiO_4)]$, all potential alteration products of spent fuel corrosion in Si-rich groundwater's [92]. The incorporation of An^{3+} into the sheets of the structures of α-uranophane and boltwoodite, as well as into interlayer sites in various uranyl phases, could occur.

The structural compatibility of the potential host phase is probably not the critical parameter determining the efficiency of retention, and many other features of the fuel corrosion/alteration process are likely to be more important. For example, if alteration involves a pseudomorphic relationship between the alteration layer and the fuel matrix the incorporation of structurally compatible radionuclides into this alteration layer might be expected to be efficient. By contrast, dissolution in grain boundaries, transport through a porous inner layer, and precipitation in a less consolidated outer layer might be expected to be a much less efficient retention process dictated by features such as local pH variations, phase solubilities, and fuel surface area to solution volume ratios. These potential influences make it important to determine whether the features of the observed spent fuel alteration process [88] are an artefact of the presence of radiation fields or a true reflection of what is to be expected in the long term fuel alteration process.

The importance of the radionuclide incorporation process is clearly demonstrated when comparing the retention of a species such as ^{237}Np under anaerobic and oxidizing conditions. Loida et al. [9] observed that this radionuclide (as well as ^{90}Sr, ^{99}Tc and ^{125}Sb) was released in proportion to its fractional fuel inventory (i.e. congruently) under anaerobic saline conditions. By contrast a substantial proportion of the ^{237}Np released was retained in alteration phases under oxidizing conditions at 90°C [85].

In a number of cases the results of experiments to determine the ability of uranium phases to retain radionuclides have been checked against solubility calculations. Quiñones et al. [93] found the concentrations of $^{241,243}Am$, $^{242,244}Cm$ and $^{154,155}Eu$ in evaporated solutions of dissolved high burn up spent fuel in 5 mol l^{-1} NaCl (pH 5.7–12) to be much lower than expected for equilibration with the solids $Am(OH)_3, Cm(OH)_3$, a clear indication that these radionuclides were coprecipitated into U (VI) phases. Loida et al. [9] performed similar calculations for Am and the rare earths. Based on fractional inventory estimates it was observed, after leaching under nominally anaerobic saline solutions (oxidizing conditions were still maintained by radiolysis), that congruent release occurred for pH < 6, but the degree of retention increased in the pH range 9–10. Since this is the pH range of minimum solubility for U(VI) phases [65], it suggests their incorporation into such phases. Solubility calculations showed the Am concentrations to be up to 10^5 times lower than expected for solubility equilibrium with $Am(OH)_3$. Further calculations showed that equilibration with solids of the form (REE; Am) $(OH)_3$ (REE – rare earth element) could not account for this factor, but coprecipitation with U(VI) phases possibly could.

While these experiments help identify the host phases for retained radionuclides, they do not necessarily produce the quantitative numbers which can be used to estimate the efficiency of retention, especially under the limited moisture conditions which will prevail at Yucca Mountain. Under these conditions, retention would be expected to be enhanced by the evaporation of stagnant solutions but retarded by the influence of convective flow. That the local transport regime is of vital importance in determining the efficiency of incorporation is clear when comparing vapour phase tests to drip tests at 90°C [85]. The ratio of U to Np in schoepite (the phase formed under moist vapour conditions) is between 1:0.003 and 1:0.006 compared to that in the original fuel which was 1:0.0005, indicating the incorporation of a large proportion of the ^{237}Np. In the drip test, the estimated U:Np in the uranyl silicate alteration phase was no greater than 1:0.0005 in the fuel, showing that retention was minor. A change in the drip rate also influenced the efficiency of retention: the cumulative release fractions for ^{239}Pu and ^{237}Pu were 10–10^2 smaller for low (0.075 ml/3.5 days) than for high (0.75 ml/3.5 days) drip rates.

It is clear from these deliberations that there is a very high probability that radionuclides, especially the actinides and rare earths, will be retained in fuel corrosion (alteration) product deposits under oxidizing conditions. This process should be efficient under stagnant, fully immersed and moist vapour conditions, but will be very dependent on transport conditions at the fuel surface. At present, insufficient evidence exists to quantify either this process or the ability of the corrosion product deposit to block fuel corrosion.

6. Review of the database of corrosion rates used in fuel modelling under Yucca Mountain conditions

The modelling and prediction of long term fuel performance requires a solid mechanistic understanding of the fuel corrosion process and a reliable database which specifies the dependence of fuel corrosion kinetics on those parameters likely to be important under repository conditions. In the previous sections an effort has been made to discuss what is known about these parameters with an emphasis on the oxidizing conditions which will prevail at Yucca Mountain. In this section a more focussed discussion on the relevance of this information to Yucca Mountain will be given. The primary aim is to determine whether the database available, and used in performance assessment models, is consistent with the wealth of published information discussed above. This database is effectively collected in Tables 2.1.3.5-4 and 2.1.3.5-5 of Ref. [3].

6.1. Intrinsic corrosion rates

The available kinetic data upon which to base model predictions have been determined using the single-pass flow-through technique. The advantages of the use of this technique in both the determination of fuel corrosion mechanisms and the measurement of reliable kinetic data were amply illustrated in the above discussions. By avoiding the complications of corrosion product deposition, the effects of various parameters and the kinetics of fuel corrosion have been measured. It has been clearly demonstrated that rates determined by this technique compare well from laboratory to laboratory [13,94]. Using this technique a systematic attempt to determine the dependence of UO_2 corrosion kinetics of pH (8–10), temperature (22–75°C), and oxygen and CO_3^{2-}/HCO_3^- concentrations (0.2–2.0 mmol l^{-1}) was undertaken and the results collected in Table 2.1.3.5–4 [3].

It is clear from the discussion of individual parameters in the above section of this report that no single mechanism of fuel corrosion applies over the full range

of the variations in these parameters. Hence, any attempt to fit the database will incorporate these inconsistencies and lead to predicted dependencies which are only approximately valid. To justify the use of such an approach it is necessary to determine whether, within the total database, the individual dependencies of fuel corrosion rate on specific parameters are consistent with known mechanisms and other published information.

6.2. Oxygen dependence

Specific differences exist in the behaviour of UO_2 and spent fuel as a function of O_2 concentration. At high carbonate concentration (20 mmol l^{-1}) and low temperature 22°C/25°C, a dependence of rate on $[O_2]$ was observed for UO_2 but not for spent fuel. For an intermediate $[CO_3]$ at (22°C/25°C) the dependence on $[O_2]$ was lower for UO_2 and absent for spent fuel. At 75°C both UO_2 and spent fuel exhibit an $[O_2]$ dependency when $[CO_3]$ is high (20 mmol l^{-1}).

Why UO_2 should show a larger dependence on $[O_2]$ than spent fuel is not clear. The results of Tait and Luht [14], Fig. 29, show a similar difference in $[O_2]$ dependence for UO_2 and spent fuel, which they attributed to the interference of radiolysis effects at low $[O_2]$. Such an argument is not easy to invoke for the data in Table 2.1.3.5-4 of the Waste Characteristics Report, since the rates of spent fuel corrosion are inevitably lower and less dependent on test variables than those for UO_2. This issue was dealt with in more detail above. It is clear from available published data that, while a different balance of kinetics appeared to exist for spent fuel and UO_2, the overall effect of this difference on the relative corrosion rates is minor. In this regard the data within the database are generally consistent with the bulk of published information. Indeed, the data in Ref. [3] provide a major contribution to the establishment of these conclusions.

6.3. pH dependence

No significant dependence of corrosion rate for either UO_2 or spent fuel is observed for pH. Admittedly, the range tested was narrow (8–10), but the lack of dependence is consistent with all other published information (Section 5.3). In this pH range the solubility of U under oxidizing conditions is independent of pH as is the composition of the fuel surface undergoing corrosion (Section 3.1). No pH dependence is to be expected until the pH falls to <6.

6.4. Carbonate dependence

It is clear from Sections 3.1.2 and 5.5 that the dependence of corrosion rate on carbonate concentration can be complex and varies with both $[O_2]$ and temperature. At a temperature of 75°C the dependence on $[CO_3]$ is lower at the low $[O_2]$ than it is at the higher concentration. This is consistent with the known mechanism of fuel corrosion in carbonate solutions. As the $[O_2]$ is decreased, the rate of oxidation of the fuel surface ($\propto [O_2]$) becomes more predominantly rate determining than the rate of UO_2^{2+} ion transfer to solution ($\propto$ to$[CO_3]$). This is clear in electrochemical experiments [35] and in single-pass flow-through experiments [14].

At 25°C, the $[CO_3]$ dependence is lower than at higher temperatures irrespective of the $[O_2]$. This is consistent with the observations of de Pablo et al. [52] who found an enhanced dependence of rate on $[CO_3]$ as the temperature increased, and showed that a change in the balance of kinetics occurred between 25°C and ~40°C. As the temperature increased control of the fuel corrosion rate shifts from the rate of surface oxidation to the rate of UO_2^{2+} ion transfer to solution.

6.5. Temperature dependence

The temperature dependence for low $[CO_3]$ is significantly less than it is for higher $[CO_3]$. This is consistent with published information which shows a much lower 'apparent' activation energy in non-complexing neutral solutions than in carbonate-containing solutions (Section 5.6). The predominant influence of carbonate is to prevent the deposition of corrosion products on the fuel surface which partially block the fuel corrosion process. However, as the temperature changes the rate determining step also changes as described above. This makes the activation energy determined in carbonate solution an 'apparent' value, and the temperature dependence remains semi-empirical despite approaching more closely to that expected for oxide dissolution processes.

6.6. Summary

It is clear from this review of the data in Table 2.1.3.5-4 of the Waste Characterization Report [3] that it is generally consistent with mechanistic understanding and published information, making it an acceptable database upon which to model spent fuel performance. The primary factors determining the corrosion rate are the intrinsic corrosion rate of the fuel, and its dependence on oxygen and carbonate concentrations and temperature. The procedures used in the development of this database are consistent with the defined ASTM standard practice [95].

7. General summary

A review of the mechanism and kinetics of nuclear fuel corrosion under waste disposal conditions has been undertaken, with a primary emphasis on conditions expected to prevail at Yucca Mountain (NV, USA).

The basic properties of UO_2 which influence its corrosion have been reviewed, including the conclusions based on electrochemical and corrosion experiments. Fuel corrosion is enhanced under oxidizing conditions, due to the much higher solubility of U^{VI} compared to that of U^{IV}. Hence, the mechanism and kinetics of reduction of both the environmentally supplied oxidant, O_2, and the radiolytically produced oxidants, H_2O_2 and radical species, were reviewed.

The influence of a wide range of parameters on fuel corrosion was discussed. These include the intrinsic corrosion rate, pre-oxidation of the fuel, pH, O_2 concentration, carbonate concentration, temperature, the effect of water radiolysis, and the formation of corrosion product deposits and their ability to both block the corrosion process and retain released radionuclides.

Finally, the database of corrosion rates in the Waste Characterization Report was evaluated in terms of the reviewed information on fuel corrosion. It was concluded that the rates in this database were generally consistent with published information, and their use in fuel degradation models justified.

Acknowledgements

This review was funded by AECL Technologies under the terms of contract #DE-AC08-95-NV 11784 with the US Department of Energy. The author is grateful to these agencies, and to Ontario Power Generation for the permission to publish many of the Figures. The author is also grateful to SKB (Stockholm, Sweden) for permission to publish Fig. 33, to Juan de Pablo (Universitat Politécnia Catalunya, Spain) for permission to reproduce the data in Fig. 11, and to John Tait for permission to reproduce Fig. 37.

References

[1] D.W. Shoesmith, F. King, B.M. Ikeda, An assessment of the feasibility of indefinite containment of Canadian nuclear fuel wastes, AECL – 10972 COG-94-534, 1995.
[2] L.H. Johnson, D.W. Shoesmith, in: W. Lutze, R.C. Ewing (Eds.), Radioactive Waste Forms for the Future, Elsevier, Amsterdam, 1988, p. 635.
[3] R.B. Stout, H.R. Leider, Waste form characteristics report, Lawrence Livemore National Laboratory Report UCRL-10-108314 Version 1.2, 1997.
[4] D.W. Shoesmith, S. Sunder, W.H. Hocking, in: J. Lipkowski, P.N. Ross (Eds.), Electrochemistry of Novel Materials, VCH, New York, 1994, p. 297.
[5] R.L. Segall, R.St.C. Smart, P.S. Turner, in: J. Nowotny, L.-C. Dufour (Eds.), Surface and Near-surface Chemistry of Oxide Materials, Elsevier Science, Amsterdam, 1988, p. 527.
[6] D.W. Shoesmith, B.M. Ikeda, F. King, S. Sunder, in: P.L. Andresen, R.N. Parkins (Eds.), Life Prediction of Structures Subject to Environmental Degradation, NACE International, Houston, TX, 1996, p. 101.
[7] S. Sunder, Alpha, beta and gamma dose rates in water in contact with used CANDU UO_2 fuel, Atomic Energy of Canada Ltd. Report, AECL-11380, COG-95-340, 1995.
[8] D.T. Reed, R.A. Van Konynenburg, Mater. Res. Soc. Symp. Proc. 112 (1988) 393.
[9] A. Loida, B. Grambow, H. Geckeis, P. Dressler, in: Proceedings of the Materials Research Society Symposium, vol. 353, Materials Research Society, Pittsburgh, PA, 1995, p. 577.
[10] I. Neretnieks, Mater. Res. Soc. Symp. Proc. 465 (1997) 574.
[11] S. Sunder, D.W. Shoesmith, M. Kolar, D.M. Leneveu, J. Nucl. Mater. 250 (1997) 118.
[12] W.J. Gray, L.E. Thomas, R.E. Einziger, Mater. Res. Soc. Symp. Proc. 294 (1993) 47.
[13] W.J. Gray, S.A. Steward, D.W. Shoesmith, J.C. Tait, in: Proceedings of the Fifth Annual International High-Level Radioactive Waste Management Conference (Waste Management '94), vol. 4, Las Vegas, Nevada, 22–26 May 1994, p. 2597.
[14] J.C. Tait, J.M. Luht, Dissolution rates of uranium from unirradiated UO_2 and uranium and radionuclides from used CANDU fuel using the single-pass flow-through apparatus, Ontario Hydro Report No. 06819-REP-01200-0006-ROO, 1997.
[15] D.W. Shoesmith, S. Sunder, M.G. Bailey, G.J. Wallace, Corros. Sci. 29 (1989) 1115.
[16] D.W. Shoesmith, S. Sunder, An electrochemistry-based model for the dissolution of UO_2, Atomic Energy of Canada Ltd. Report, AECL – 10488, 1991.
[17] J. de Pablo, J. Gimenez, M.E. Torrero, I. Casas, Mater. Res. Soc. Symp. Proc. 353 (1995) 609.
[18] J. de Pablo, I. Casas, J. Gimenez, V. Marti, M.E. Torrero, J. Nucl. Mater. 232 (1996) 138.
[19] J.L.M. Luht, M.Sc. thesis, University of Manitoba, Winnipeg, 1998.
[20] J.D. Rudnicki, R.E. Russo, D.W. Shoesmith, J. Electroanal. Chem. 372 (1994) 63.
[21] Hj. Matzke, A. Turos, Solid State Ionics 49 (1991) 189.
[22] Hj. Matzke, J. Nucl. Mater. 238 (1996) 58.
[23] J.S. Betteridge, N.A.M. Scott, D.W. Shoesmith, L.E. Bahen, W.H. Hocking, P.G. Lucuta, Effects of hyperstoichiometry and fission products on the electrochemical reactivity of UO_2 nuclear fuel, Atomic Energy of Canada Ltd. Report, AECL – 11647, COG-96-331-I, 1997.
[24] W.J. Gray, D.M. Strachan, Mater. Res. Soc. Symp. Proc. 212 (1991) 205.
[25] R.E. Einziger, L.E. Thomas, H.C. Buchanan, R.B. Stout, J. Nucl. Mater. 190 (1992) 53.
[26] S. Sunder, L.K. Strandlund, D.W. Shoesmith, Electrochim. Acta 43 (1998) 2359.
[27] D.W. Shoesmith, F. King, A mixed-potential model for the prediction of the effects of alpha-radiolysis, precipitation and redox processes on the dissolution of used nuclear fuel, Ontario Hydro Report, 06819-REP-01200-MPM R00, 1998.
[28] S. Sunder, D.W. Shoesmith, R.J. Lemire, M.G. Bailey, G.J. Wallace, Corros. Sci. 32 (1991) 373.
[29] P.D.W. Bottomley, D.H. Wegen, M. Coquerelle, J. Nucl. Mater. 238 (1996) 23.

[30] M.J. Nicol, C.R.S. Needes, The mechanism of the anodic dissolution of uranium dioxide, National Institute for Metallurgy, Republic of South Africa, Report No. 7079, 1973.
[31] M.E. Torrero, E. Baraj, J. de Pablo, J. Gimenez, I. Casas, Int. J. Chem. Kinet. 29 (1997) 261.
[32] I. Casas, J. Gimenez, J. de Pablo, M.E. Torrero, Mater. Res. Soc. Symp. Proc. 294 (1993) 67.
[33] I. Grenthe, D. Fein, F. Salvatore, G. Riccio, J. Chem. Soc. Dalton Trans. 11 (1984) 2439.
[34] D.W. Shoesmith, S. Sunder, M.G. Bailey, G.J. Wallace, F.W. Stanchell, Appl. Surf. Sci. 20 (1984) 39.
[35] D.W. Shoesmith, S. Sunder, M.G. Bailey, G.J. Wallace, F.W. Stanchell, Appl. Surf. Sci. 20 (1984) 39.
[36] S. Sunder, D.W. Shoesmith, H. Christensen, N.H. Miller, J. Nucl. Mater. 190 (1992) 78.
[37] D.W. Shoesmith, S. Sunder, L.H. Johnson, M.G. Bailey, Mater. Res. Soc. Symp. Proc. 50 (1985) 309.
[38] S. Sunder, D.W. Shoesmith, N.H. Miller, J. Nucl. Mater. 244 (1997) 66.
[39] D.W. Shoesmith, S. Sunder, M.G. Bailey, N.H. Miller, J. Nucl. Mater. 227 (1996) 287.
[40] D.W. Shoesmith, W.H. Hocking, S. Sunder, J.S. Betteridge, N.H. Miller, J. Alloy Comp. 213&214 (1994) 551.
[41] W.H. Hocking, J.S. Betteridge, D.W. Shoesmith, The cathodic reduction of oxygen on uranium oxide in dilute aqueous solution, Atomic Energy of Canada Ltd. Report, AECL – 10402, 1991.
[42] E.J.M. O'Sullivan, E.J. Calvo, in: Electrode Kinetics, in: R.G. Compton (Ed.), Comprehensive Chemical Kinetics, vol. 27, Elsevier, Amsterdam, 1987, p. 247 (Chapter 3).
[43] V.A. Presnov, A.M. Trunov, Electrokhimiya 11 (1975) 77.
[44] W.H. Hocking, J.S. Betteridge, D.W. Shoesmith, J. Electroanal. Chem. 379 (1994) 339.
[45] H. Christensen, R. Forsyth, R. Lundquist, L.O. Werme, Radiation induced dissolution of UO_2, Studsvik Energiteknik Report NS-90/85, 1990.
[46] C.R.S. Needes, M.J. Nicol, A study of some redox reactions at a UO_2 surface, National Institute for Metallurgy, Republic of South Africa, Report No. 7073, 1973.
[47] J. Gimenez, E. Baraj, M.E. Torrero, I. Casas, J. de Pablo, J. Nucl. Mater. 238 (1996) 64.
[48] P. Diaz-Arocas, J. Quinones, C. Maffiotte, J. Serrano, J. Garcia, J. Almazan, J. Esteban, Mater. Res. Soc. Symp. Proc. 353 (1995) 641.
[49] H. Christensen, S. Sunder, D.W. Shoesmith, Development of a kinetic model to predict the rate of oxidation and dissociation of nuclear fuel (UO_2) by the radiolysis of water, Atomic Energy of Canada Ltd. Report, AECL – 11102, COG-93-488, 1994.
[50] M.G. Bailey, L.H. Johnson, D.W. Shoesmith, Corros. Sci. 25 (1985) 233.
[51] J.C. Wren, S. Sunder, D.W. Shoesmith, A finite element model to predict the concentration of radiolysis products in narrow gaps, Ontario Hydro Report, 1998.
[52] J. de Pablo, I. Casas, J. Gimenez, M. Molera, M.E. Torrero, Mater. Res. Soc. Symp. Proc. 465 (1997) 535.
[53] J. Bruno, I. Casas, E. Cera, J. de Pablo, J. Gimenez, M. Torrero, Mater. Res. Soc. Symp. Proc. 353 (1995) 601.
[54] S.A. Steward, E.T. Mones, Mater. Res. Soc. Symp. Proc. 465 (1994) 557.
[55] W.J. Gray, L.E. Thomas, Mater. Res. Soc. Symp. Proc. 333 (1994) 391.
[56] B.D. Hanson, The burn up dependence of light water reactor spent fuel oxidation, Pacific Northwest National Laboratory Report, PNNL-11929, 1998.
[57] E. Siegmannn, Cladding Credit in TSPA-VA, Presented at the Waste Forms Degradation Expert Elicitation Meeting, San Francisco, 15–16 December 1997.
[58] L.H. Johnson, P. Taylor, Alteration of spent CANDU fuel in aerated steam at 150°C, Atomic Energy of Canada Ltd. Report, 1999, to be published.
[59] P. Taylor, D.D. Wood, A.M. Duclos, D.G. Owen, J. Nucl. Mater. 168 (1989) 70.
[60] P. Taylor, D.D. Wood, D.G. Owen, W.G. Hutchings, A.M. Duclos, Microstructures and phase relationships of crystalline oxidation products formed on unused CANDU fuel exposed to aerated steam and aerated water near 200°C, Atomic Energy of Canada Ltd. Report, AECL – 10476, COG-91-292, 1991.
[61] P. Taylor, D.D. Wood, D.G. Owen, J. Nucl. Mater. 223 (1995) 316.
[62] K.M. Wasywich, W.H. Hocking, D.W. Shoesmith, P. Taylor, Nucl. Technol. 104 (1993) 309.
[63] W.J. Gray, Spent fuel dissolution rates as a function of burn up and water chemistry, Pacific Northwest National Laboratory Report, PNNL-11895, UC-802, 1998.
[64] I. Perez, I. Casas, M.E. Torrero, E. Cera, L. Duro, J. Bruno, Mater. Res. Soc. Symp. Proc. 465 (1997) 565.
[65] I. Grenthe, J. Fuger, R.J.M. Konings, R.J. Lemire, A.B. Muller, C. Nguyen-Trung, H. Wanner, Chemical Thermodynamics of Uranium, in: H. Wanner, I. Forest (Eds.), Chemical Thermodynamics, vol. 1, North-Holland, Amsterdam, 1992.
[66] G.F. Thomas, G. Till, Nucl. Chem. Waste Manage. 5 (1984) 141.
[67] S.A. Steward, H.C. Weed, Mater. Res. Soc. Symp. Proc. 333 (1997) 409.
[68] B. Grambow, A. Loida, P. Dressler, H. Geckeis, J. Gago, I. Casas, J. de Pablo, J. Gimenez, M.E. Torrero, Long-term safety of radioactive waste disposal: chemical reaction of fabricated and high burn up spent UO_2 fuel with saline brines, Wissenschaftliche Berichte FZKA 5702, Technik und Umwelt, Forschungszentrum Karlsruhe, 1996.
[69] D.E. Grandstaff, Econ. Geol. 71 (1976) 1493.
[70] S.A. Steward, W.J. Gray, in: Proceedings of the Fifth International Conference on High-Level Radioactive Waste Management, American Nuclear Society, La Grange Park, IL, 1994, p. 2602.
[71] J.B. Hiskey, Inst. Min. Metall. Trans. Sect. C 88 (1979) C145.
[72] J.B. Hiskey, Inst. Min. Metall. Trans. Sect. C 89 (1980) C145.
[73] G.I. Park, H.K. Lee, J. Korean Nucl. Soc. 28 (1996) 349.
[74] M.-P. Lahalle, R. Guillamont, G.C. Allen, J. Chem. Soc. Faraday Trans. 86 (1990) 2641.
[75] A.Y. Plyasunov, I. Grenthe, Geochim. Cosmochim. Acta 58 (1994) 3561.
[76] I.G. Gorichev, N.A. Kyprianov, Russ. Chem. Rev. 53 (1984) 1039.
[77] V. Gromov, Radiat. Phys. Chem. 18 (1981) 135.

[78] A. Loida, B. Grambow, H. Geckeis, J. Nucl. Mater. 238 (1996) 11.
[79] P.A. Finn, J.K. Bates, J.C. Hoh, J.W. Emery, L.D. Hafenrichter, E.C. Buck, M. Gong, Mater. Res. Soc. Symp. Proc. 333 (1994) 399.
[80] P.A. Finn, E.C. Buck, J.C. Hoh, J.K. Bates, in: International Conference on Evaluation of Emerging Nuclear Fuel Cycle Systems, Versailles, France, 11–14 September 1995, p. 241.
[81] P.A. Finn, J.C. Hoh, S.F. Wolf, M.T. Surchik, E.C. Buck, J.K. Bates, Mater. Res. Soc. Symp. Proc. 465 (1997) 527.
[82] P.-M. Heppner, D. Wegen, G. Marx, Radiochim. Acta 58&59 (1992) 21.
[83] W.J. Gray, L.E. Thomas, in: Proceedings of the Third International Conference on High-Level Radioactive Waste Management, American Nuclear Society, La Grange Park, IL, 1992, p. 1458.
[84] S. Stroes-Gascoyne, L.H. Johnson, J.C. Tait, J.L. McConnell, R.J. Porth, Mater. Res. Soc. Symp. Proc. 465 (1997) 511.
[85] E.C. Buck, R.J. Finch, P.A. Finn, J.K. Bates, in: Proceedings of the Materials Research Society Symposium, vol. 506, Materials Research Society, Pittsburgh, PA, 1998, p. 87.
[86] E.C. Buck, D.J. Wronkiewicz, P.A. Finn, J.K. Bates, J. Nucl. Mater. 249 (1997) 70.
[87] C.N. Wilson, W.J. Gray, Mater. Res. Soc. Symp. Proc. 176 (1990) 489.
[88] D.J. Wronkiewicz, J.K. Bates, S.F. Wolf, E.C. Buck, J. Nucl. Mater. 238 (1996) 78.
[89] D.J. Wronkiewicz, E.C. Buck, J.K. Bates, Mater. Res. Soc. Symp. Proc. 465 (1997) 519.
[90] P.C. Burns, R.J. Finch, F.C. Hawthorne, M.L. Miller, R.C. Ewing, J. Nucl. Mater. 249 (1997) 199.
[91] P.C. Burns, R.C. Ewing, M.L. Miller, J. Nucl. Mater. 245 (1997) 1.
[92] D.J. Wronkiewicz, J.K. Bates, T.J. Gerding, E. Veleckis, B.S. Tani, J. Nucl. Mater. 190 (1992) 107.
[93] J. Quiñones, B. Grambow, A. Loida, H. Geckeis, J. Nucl. Mater. 238 (1996) 38.
[94] D.W. Shoesmith, J.C. Tait, S. Sunder, W.J. Gray, S.A. Steward, R.E. Russo, J.D. Rudnicki, Factors affecting the differences in reactivity and dissolution rates between UO_2 and spent nuclear fuel, Atomic Energy of Canada Ltd. Report, AECL – 11515, COG-95-581, 1996.
[95] ASTM Standard practice for prediction of the long-term behaviour of materials, including waste forms, used in engineered barrier systems (EBS) for geological disposal of high-level active waste, ASTM designation: C 1174-97, ASTM, West Conshohocken, PA, 1998.